Personalised 3D Assessment of Trochanteric Soft Tissues Improves HIP Fracture Classification Accuracy

Energy Efficiency (2024) 17:95
https://doi.org/10.1007/s12053-024-10266-1

ORIGINAL ARTICLE

Wind-driven and buoyancy effects for modeling natural ventilation in buildings at urban scale

Silvia Santantonio · Oronzo Dell'Edera · Claudio Moscoloni · Cristina Bertani · Giovanni Bracco · Guglielmina Mutani

Received: 21 July 2023 / Accepted: 6 October 2024

Abstract This work proposes a new model to evaluate the air changes per hour (ach) due to natural infiltrations in buildings. This modeling already exists at building scale, but the new model will implement the hourly ventilation load in a physical-based modeling for space heating and cooling in buildings at urban scale. The proposed improvement considers the wind and buoyancy effects in the calculation of hourly achs in a high-density urban context. A three-zone air flow lumped modeling is applied to describe the air flow in buildings; the air flow rate due to infiltrations is calculated depending only on leakages' characteristics and pressure variations in various climate conditions. The non-linear equations system of mass and energy conservation is solved by an iterative procedure using the Newton-Raphson numerical method. Besides, two different methodologies are compared to evaluate the external dynamic and static pressure conditions on building façades: experimental values (pressure coefficients Cp) and CFD simulations. For the latter, the air flow field in the urban canyons is described by the windy conditions and by imposing a temperature gradient due to solar irradiation between the windward and leeward facades. This methodology is applied to three urban canyons in Turin, with typical aspect ratios and orientations for some local climate conditions considering both heating and cooling seasons. Comparing the results of hourly ach obtained from the Cp method, the CFD technique allows to modulate the ach considering the impact of the canyon dimension, wind and buoyancy effect of non-isothermal condition, in varying the wind speed on the façades of buildings for different scenarios. It also overcomes the limit of field of applications of Cp, especially in high-density built urban environments. The encouraging results of this work will lead to future developments of the three-zone lumped model and its numerical solution techniques.

Keywords Natural ventilation · Leakages · Wind driven effect · Thermal buoyancy effect · Air changes per hour · Lumped parameter model · Numerical method · CFD · Pressure coefficient Cp · Urban canyon · Urban building energy modeling

S. Santantonio · C. Bertani · G. Mutani (✉)
DENERG Politecnico di Torino, corso Duca degli Abruzzi 24, 10129 Torino, Italy
e-mail: guglielmina.mutani@polito.it

O. Dell'Edera · C. Moscoloni · G. Bracco
DIMEAS Politecnico di Torino, corso Duca degli Abruzzi 24, 10129 Torino, Italy

C. Moscoloni
University School for Advanced Studies IUSS Pavia, piazza della Vittoria 15, 27100 Pavia, Italy

Nomenclature

Symbols and units		
ach		Air changes per hour 1/h
A		Area m^2
Cd		Discharge Coefficient -
Cp		Pressure Coefficient -
	alt	Altitude m (asl)

Published online: 12 November 2024

$DirV$	Wind direction (undisturbed flow) 0°(N)
g	Gravity m/s^2
H	Height of the canyon m
he	Convective exchange capacity W/m^{2}K
H/W	Aspect ratio (Height-to-Width) -
K	Leakage coefficient -
I_b	Direct normal solar irradiation W/m^2
I_d	Diffuse solar irradiation W/m^2
I_{inc}	Incident solar irradiation W/m^2
$\dot{m}$	Air flow rate Kg/s
n	Type of flux motion (coeff.) -
P_{atm}	Atmospheric pressure Pa
p_{dyn}	Dynamic pressure Pa
p_s	Static pressure Pa
p_{pot}	Potential pressure Pa
T_{air}	Air temperature °C, K
$T_{s\text{-}a}$	Sol-air temperature °C, K
U	Wind velocity (undisturbed flow) m/s
v	Wind velocity (inside canyon) m/s
vol	Volume m^3
W	Width of the canyon m
z	Height from the ground m
α	Absorption factor -
β	Sun incident angle on building facade °
ΔP	Pressure variation between nodes Pa
ΔT	Temperature variation inside canyon K
θ	Wind direction (undisturbed flow) 0°(N)
υ	Roughness parameters -
ρ	Air density Kg/ m^3
Subscripts C	Celsius degree
i	generic node
L	links associated to a node
op	opening
ref	reference
$1, 2, 3, 4$	external nodes
$a', a'', b', b'', c', c'', c''', c^v$	internal nodes at leakage level
K	Kelvin degree
in	internal/indoor
leak	leakage
out	outdoor
sh	shaft
a,b,c	Internal nodes and zones
Acronyms GHG	Green House Gases
GIS	Geographic Information System
HVAC	Heating, Ventilation and Air Conditioning
RES	Renewable Energy Sources
SVF	Sky View Factor
UBEM	Urban Building Energy Modeling
WCF	Windward Cold Façade
WWF	Windward Warm Façade

Introduction

Energy planning is becoming crucial to face current challenges: crisis of energy prices, war, pandemic, and climate change (Perera et al., 2023). Many countries and cities around the world are developing plans and strategies to reach an ever-greater level of energy self-sufficiency and carbon-neutrality (https://resilientcitiesnetwork.org).

In, high-density urban contexts, where the energy consumption for buildings space heating predominantly contributes to GHG emissions, these goals are even more difficult to reach due to a spatial coexistence of high-energy intensity and low availability of renewable energy sources (RES) (Mutani et al., 2023). This challenge requires pursuing and boosting energy policies to reduce and optimize consumption, but also broadening the energy assessments at the territorial scale, including the spatial and temporal dimension.

The complexity of this issue consistently increases in the attempt of describing local phenomena and managing their mutual influence with larger scale phenomena, with many random factors as the one related to energy use (Perera et al., 2021). Reliable energy models and tools are necessary based on accessible databases to be easily replicable in any

context and scale (Palusci & Cecere, 2022). In addition, to evaluate the impact of each intervention on the overall energy performance of a building, it is no longer useful to implement energy assessments for single buildings and their contexts, but rather to consider the interdependent system of buildings that make up homogeneous areas in the city as the object of investigation (Basu et al., 2019).

The assessment of urban ventilation is a clear example of a phenomenon that varies in relation to the scale and has a strong mutual influence with the spatial and geometric characteristics of urban obstacles (buildings). Urban morphology affects urban ventilation which reciprocally influences the ventilation inside or through buildings and consequently their energy demand (Rezaeiha et al., 2020).

State of the art

Urban building energy modeling

Many literature reviews (Ali et al., 2021), (Harish & Kumar, 2016) describe existing Urban Building Energy Modeling (UBEM) referring to their different approaches (bottom-up or top-down) and their modeling type (data-driven, process driven or hybrid).

Physical-based engineering models are used to assess the energy performance of buildings, evaluating separately how each thermal gain (or loss) affects the thermal energy balance equation for building space heating (or cooling). A topic of recent debate is their implementation with a place-based approach. This can help in defining proper solutions, suitable for each specific case study (Mutani et al., 2023). Its potentiality origins from relying on wide available geo-databases and interoperable tools (i.e., GIS) which facilitate the description of spatial relationship between elements and the interchange between the spatial scale of energy analysis: from the building to the block-district-city and territorial scales. In this way it is possible to evaluate the effect of each single intervention and its repercussions on systems correlated to it.

This work is part of a broader research activity whose main objective is the implementation of an already existing place-based engineering urban energy model for the assessment of the monthly-hourly space heating and cooling energy consumption of residential building both at building and urban scale, to which apply the hourly variation of ach (Mutani & Todeschi, 2020).

Ventilation assessment at building level

Regarding the heat flow rate by ventilation in the assessment of the thermal energy balance equation for the space heating and cooling of residential buildings, the main parameter is the air change per hour (ach). As reported in (Mutani et al., 2021), it mainly depends on the air flow rate through a building and its volume. Concerning only the air flow due to infiltrations of openings, the infiltration rate is caused by pressure difference generated by the incident wind on building façades and the thermal buoyancy inside building zones. It depends also on the airtightness of the building envelope and its components. In scientific literature, natural ventilation at building level has been deeply investigated for different studies concerning indoor air quality, including fire safety (Calì et al., 1997), HVAC, and energy performance efficiency.

The most frequent methods used in the scientific literature to assess the infiltration rate and the ach are:

- measurements and field experiments, testing the permeability of single technological components; ach is then derived and tabular data are created for class of building typology and pressure difference (Mun et al., 2021);
- network-based multizone models to compute the interaction of airflow between different zones on a whole-building scale. Knowing the local values for the input variables and assuming some stringent boundary conditions, it is possible to apply physical equations of fluid dynamics phenomena to determine the output parameters in all zones of the network. Model's computational effort increases with the complexity of the network elements. The most used parametric models are CONTAM (Dols & Polidoro, 2020) and COMIS (Feustel, 2013);
- Computational Fluid Dynamic models (CFD) are based on differential equations of energy, mass, and momentum to determine airflows over time on a detailed grid describing model geometry. High computational cost and high case-dependency (Najafi et al., 2023) make it less appropriate for large-scale building analyses.

In this work, a lumped parameters network-based multizone model is applied to calculate the ach at building level. It represents a good compromise for the description of the physical phenomena, the number of input variables, the detail of the characteristics of the building, whose schematic description is simple enough to apply the model's balance equations to all the buildings in an urban area.

Ventilation assessment at urban level

Ventilation within urban street canyon is acquiring importance in the scientific framework due to its impact in heat stress exposure, pollutants and increasing energy demand. Among different methods to study how the wind profile is influenced by the presence of roughness elements (buildings), in (Santantonio & Mutani, 2022) a GIS-based methodology and open-source QGIs plug-in are used to adjust the wind velocity above the displacement layers (Fig. 1a, b). The GIS tool is based on Digital Surface Modeling (DSM) that easily described the real urban built environment and spatial relationship between objects. The height of displacement layer *zd* is assessed as a function of morphometric parameters (i.e., Building Density, building height variability, Frontal Area Index), for each specified wind directions representative of the local climate; results are referred to a predefined grid at urban scale to describe the spatial distribution of *zd*. Knowing the height of the displacement layer *zd* in front of each building, a wind profile is assigned to every building of the examined area. In this way it is possible to indicate in which urban canyons turbulent flows are generated (Fig. 1b). Compared to parametric models based on tabular data with limited fields of application (i.e., υ roughness parameters), a GIS-based modeling can determine wind profiles at urban scale considering the real characteristics, size and geometry of all the objects (buildings) and the exact spatial relationships of urban canyons, for each examined wind direction. The displacement layer (zd) can be intended as a threshold value (Fig. 1a):

- above zd the reference speed of the undisturbed wind is corrected by applying the logarithmic law and calculating it directly in GIS on an urban scale;
- below zd the turbulent motion generates vortexes and eddies, which can only be investigated using CFD models to be applied to canyons with similar characteristics.

2D CFD urban canyon model

In the reference scientific literature of urban microclimate studies, numerical solutions relying on CFD simulations are acquiring importance. In the field of

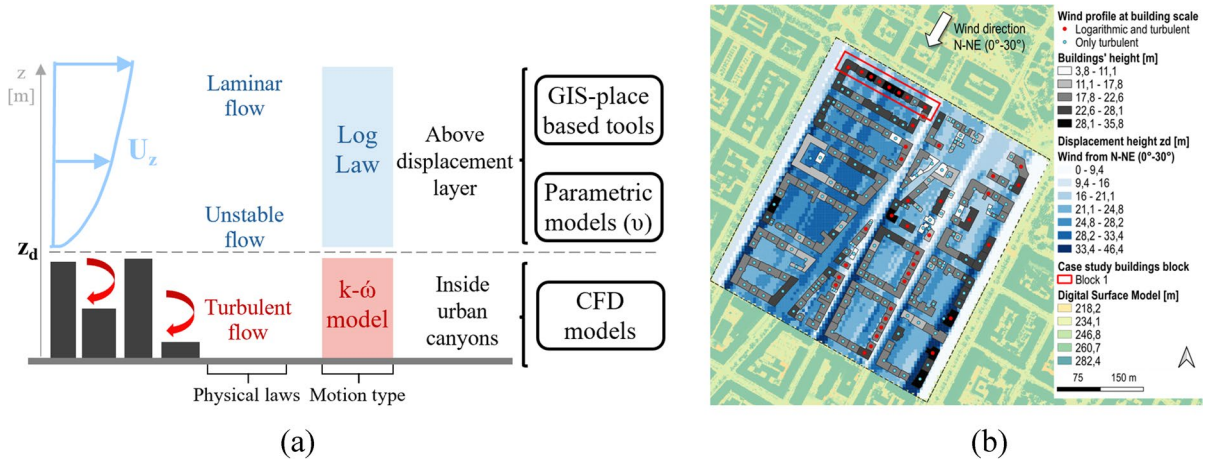

Fig. 1 The displacement layer zd as a threshold value to identify wind profiles and modeling type (**a**) at urban level, and and an example of the result of the spatial distribution of the parameter zd at an urban scale evaluated with a GIS-based model and plugin (**b**)

urban ventilation studies, they provide many advantages: variables are investigated in the entire computational domain, simulations explicitly perform the coupling of wind velocity and temperature fields, even at finer scales. A review on the CFD analysis of urban microclimate (Toparlar et al., 2017) reports several CFD studies at the building scales, concerning natural ventilation and wind flows around buildings: many of these adopt 2D modeling focusing on urban street canyons (Li et al., 2012), with the possibility of coupling CFD analysis and building energy simulations to evaluate the building energy consumption (Bartak et al., 2002). The mentioned review investigates and categorizes all CFD studies based on the type of urban area (real or generic) and the presence of validation. The result shows that the majority of studies concerns real urban areas conducted without validation, using RANS equations; generally, they consist of comparative studies among different configurations in the same urban area with the aim to optimize target variables. The lack of CFD validation is explained by the common difficulty in finding relevant or well-documented measured data: measurement campaigns on urban areas imply logistic challenges and data quality issues. Even if it requires further investigation, a possible solution to these difficulties may be represented by the great availability of data detectable by the Internet of Things, using low-cost environmental sensors with WiFi network, that are increasingly widely distributed in urban areas.

Many simplified models are used to compose building geometries forming urban structures. The choice between 2D or 3D urban canyon models is based on the features of the phenomenon investigated (i.e., wind speed, pollutant dispersion, etc.), and the scale of interests. It can imply specific morphometric parameters as input data: in 2D models the most used are the *aspect ratio* and *building height* or *height variation*, in 3D models *length-to-width* or *length-to-high*, and *plan area density* are fundamental (Palusci et al., 2022). Two-dimensional (2D) urban models have been applied to study the impact of the urban canyon aspect ratio on urban ventilation and pollutant dispersion (Di Bernardino et al., 2018). Most studies apply 3D CFD model on generic building geometries that form idealized urban structures (Ai & Mak, 2017). Studies on actual urban areas are still rare due to the complexity of describing the physical phenomena and the high level of detail required in modeling the built environment. More frequently the aim of these studies is to describe phenomena in specific contexts (Tsichritzis & Nikolopoulou, 2019), verify the accuracy of the computational settings (O'Neill et al., 2016) or evaluate the correlation between urban parameters and wind speed (Palusci & Cecere, 2022). (Javanroodi et al., 2022) highlighted the difficulty in generalizing the results of the 3D CFD simulations and propose two data-driven models to downscale climate variables at defined urban forms, considering extreme climate conditions. As described in the Best Practice Guidance (BPG) on CFD analysis for wind comfort and safety (Blocken et al., 2012), all buildings relevant for the wind should be modeled explicitly; but this requirement cannot be easily achieved for neighborhood-scale applications for a whole city. Nevertheless, the neighborhood scale is considered the best compromise for describing the entire physical process of natural ventilation and the actual urban configuration that influences it (Sanaieian et al., 2014).

A lack of investigation of CFD simulations regards the evaluation of urban airflows pattern in non-isothermal conditions, considering the combined effect of cross wind and thermal gradient in urban street canyons. (Mouzourides et al., 2022) deepen this topic through experimental investigation and corresponding 2D CFD analysis used to acquire velocity vector field in examined canyons of different aspect ratio. Results show that aspect ratio affects velocity field and vortical structure whose flow direction is influenced also by the presence of heated walls.

In this paper, the choice of the 2D CFD scheme is dictated by the aim to define a methodology at neighborhood scale to investigate the physical phenomena of crosswind driven and thermal gradient in the urban canyons (UC), with a sufficiently acceptable level of accuracy to apply the simulation results to similar areas within the city. The authors chose to analyze the ideal case of the urban canyon of infinite length to limit the number of parameters, as it alone allows to characterize the canyon geometry. In case of a dense, compact, and regular built environment, urban street canyons are easily assumed to be an infinite canyon; the 2D CFD scheme is a representative vertical section of the entire infinite canyon and is considered sufficient to describe the variables that influence the physical phenomena evaluated in the project

study. In this study, 3D CFD modeling would add a higher level of description of reality, but in addition to the computational effort required, it would not solve the difficulty of making the results replicable at city scale.

Research objectives

The main objectives of this paper consist in:

- 2D CFD simulations to study the velocity field of wind inside urban canyons, describing relation between environmental conditions and canyon dimensions, considering combined cross natural wind and thermal gradient, and evaluating their contributions.
- Describing the 3-zone air flow lumped parameter model to calculate the hourly air change per hour as a function of environmental conditions and building characteristics.
- Comparing different results of hourly ach applying tabular data of pressure coefficient (Cp) or the wind velocity field inside urban canyon from CFD simulations in the calculation of the dynamic pressure incident on the building windward façade.

Materials and method

The input data regarding local climate, urban morphology and building characteristics have been harmonized using Q-GIS software and, then a unique geo-database has been created. It has been applied in the two main steps that made up the overall methodology of this work, as synthetized in Fig. 2: the investigation of the air flow at urban and building scale. In the first step, CFD simulations have been done to study the velocity field of wind and vortical structures in the domain of urban canyons; the final output is the wind velocity *v*, calculated as a function of the height *(z)* from the ground in the canyon and it is used as an input data in the 2nd step of analysis. The second step consists of the application of a 3-zone air flow model to calculate the ach in several environmental conditions. This model is then used to compare 2 different methods in the calculation of the dynamic pressure (P_{dyn}) incident on the building facades.

Ventilation assessment in the urban street canyon

To investigate the phenomena involved in the ventilation assessment in the urban street canyon, a CFD model has been developed. The CFD model

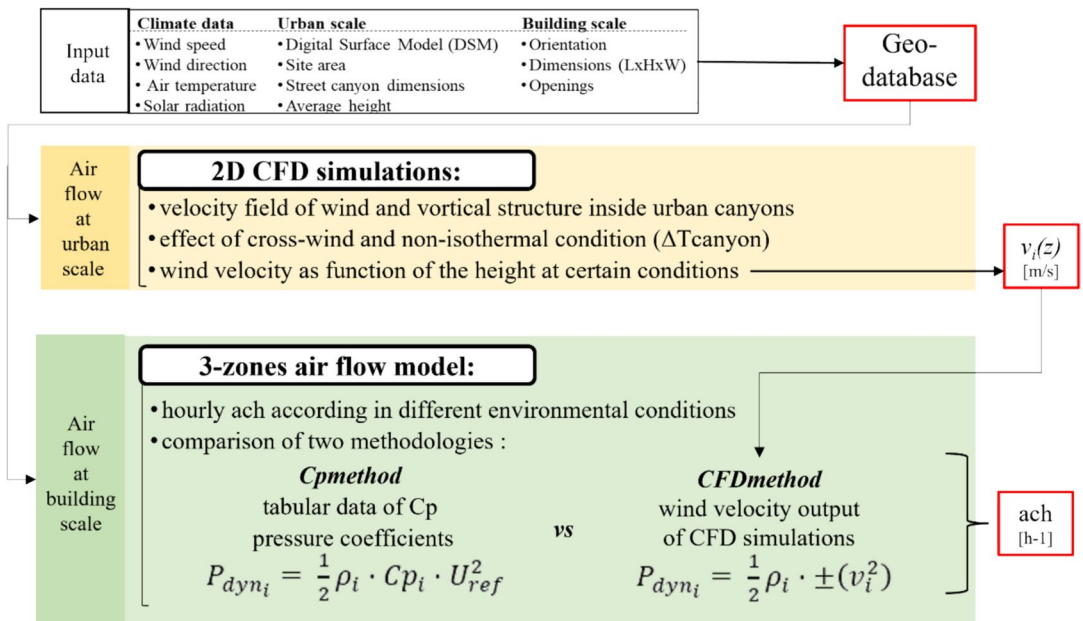

Fig. 2 Flowchart of the methodology

employed in this study utilizes the Star CCM+ software, version 2310.

The model is designed to investigate wind and heat transfer phenomena within an urban canyon. In the reference scientific literature, the RANS (Reynolds-Averaged Navier-Stokes) approach is the most widely used to conduct numerical simulations, assuming a steady state flow regime; it also considered an optimal compromise for efficiency and accuracy of building-terrain solving local climate studies (Javanroodi et al., 2022). The k-ω turbulence model has been selected for this study due to its effectiveness in capturing flow characteristics around buildings, offering good predictive capabilities for both the near-wall and free-stream regions (Ai & Mak, 2017). This model assumes a steady state flow regime, which is appropriate given the primarily steady conditions expected in the study area and the practical need for reasonable computational times.

Boundary conditions of the domain The physical domain has been mapped using a combination of structured and unstructured elements; the structured mesh is employed in the regions where the geometry allows for a regular grid, such as the main urban canyon section. This structured mesh provides good resolution and efficient computation. However, specific urban canyon regions, characterized by high flow gradients such as corners, have been refined to capture the local flow complexity.

To study separately the contribution of thermal gradient and cross natural wind in determining the velocity field in the domain, the input parameters used are the following (also schematized in Fig. 2a, b):

- the geometry of the urban canyon described by the aspect ratio parameter *H/W*, where *H* [m] is the average height of the buildings and *W* [m] is the width of the street; the canyon length is usually considered regular and infinite (Samsonov et al., 2015) and the main direction is here defined as θ [°] (0°N-clockwise);
- the local climate condition of reference wind speed U_{ref} [m·s^{-1}], necessarily perpendicular to the canyon axis direction, and temperature variation (ΔT).

Validation of the model and grid convergence To validate the CFD model, we reproduced test cases from an experimental campaign (Allegrini et al., 2013), and (Allegrini et al., 2014). In the experimental campaign, a wind tunnel setup was used to simulate the flow within an urban street canyon. The physical model had dimensions W×H×L=20×20×180, with the airflow directed perpendicular to the canyon's longitudinal axis. The canyon surfaces, made of aluminum, provided a smooth, low-roughness environment, allowing us to ignore surface roughness in the numerical model. The walls and ground were heated uniformly using mats, ensuring consistent temperature distribution due to aluminum's high thermal conductivity. Particle Image Velocimetry (PIV) was employed to measure flow characteristics, focusing on a central cross-section of the canyon.

For the grid convergence study, simulations were conducted with four different base mesh sizes (BS) under isothermal conditions (U_{ref} 1.45 [m·s^{-1}] T_{ref} 23 [°C]). Figure 3a and b present the normalized vertical velocity along the horizontal centerline and the normalized horizontal velocity along the vertical centerline of the canyon, respectively. These figures compare the experimental data with numerical results from each mesh size. The normalized vertical velocity profiles (Fig. 3a) and the horizontal velocity profiles (Fig. 3b) showed minimal differences among the three finest meshes (BS 1, BS 2, and BS 4), indicating good agreement with experimental data.

Table 1 below reports the Normalized Root Mean Square Error (NRMSE) for the isothermal case, calculated using the following formula in Eq. (1):

$$NRMSE = \frac{\sqrt{\frac{\sum_{i=1}^{N}(y_1 - y_2)^2}{N}}}{\max(y_1) - \min(y_1)} \quad (1)$$

where y_1 represent the experimental data and y_2 the data obtained with the numerical model. (Allegrini et al. 2013, 2014).

Given the results of the grid convergence, the BS 4 was chosen for subsequent simulations, providing a balance between accuracy and computational efficiency. Figure 4 provides a visual comparison of the normalized velocity fields inside the canyon, demonstrating the numerical model's capability to accurately represent the velocity distribution.

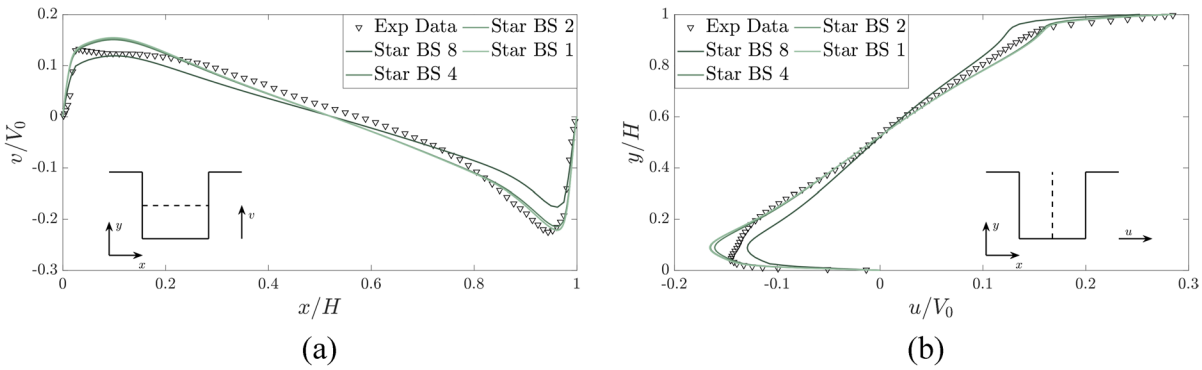

Fig. 3 In black the velocity measured in the experimental campaign. In green the results obtain with the numerical model for 4 different Base Size (BS). Both axes have been normalized

Table 1 NRMSE for the isothermal case

Mesh Base Size	N° of cell	NRMSE Vy (Fig. 3a)	NRMSE Vx (Fig. 3b)
BS 8	30K	0.0694	0.0472
BS 4	85K	0.0497	0.0258
BS 2	250K	0.0503	0.0259
BS 1	760K	0.0506	0.0262

Further validation was performed for scenarios with a windward warm facade. Four different temperature differences were tested with U_{ref} 2.32 [m·s^{-1}], and normalized horizontal velocity were compered along the canyon centerline with experimental data (Fig. 5). The agreement between the simulated and measured data further corroborated the model's reliability in presence of a thermal gradient.

Steady State and Unsteady differences To assess the differences between steady-state (RANS) and unsteady (URANS) simulations, we performed a comparative analysis on the isothermal case, using identical boundary conditions and numerical settings across both models. The only variation was the introduction of temporal dynamics in the URANS model. The simulation has a dt of 0.04s and it is 20s long. The results shown represent the mean values and the standard deviation of

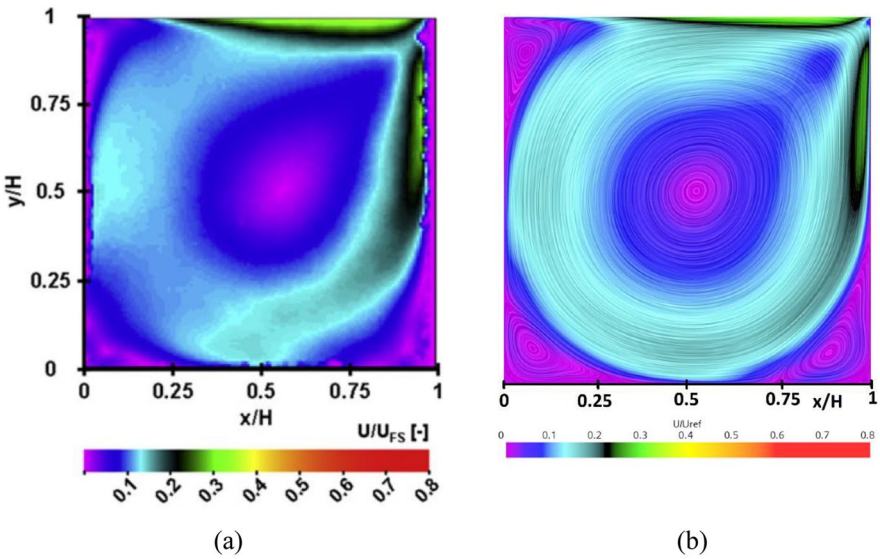

Fig. 4 Normalized velocity inside the canyon. On the left the experimental campaign. On the right the numerical model developed (Allegrini et al. 2013, 2014)

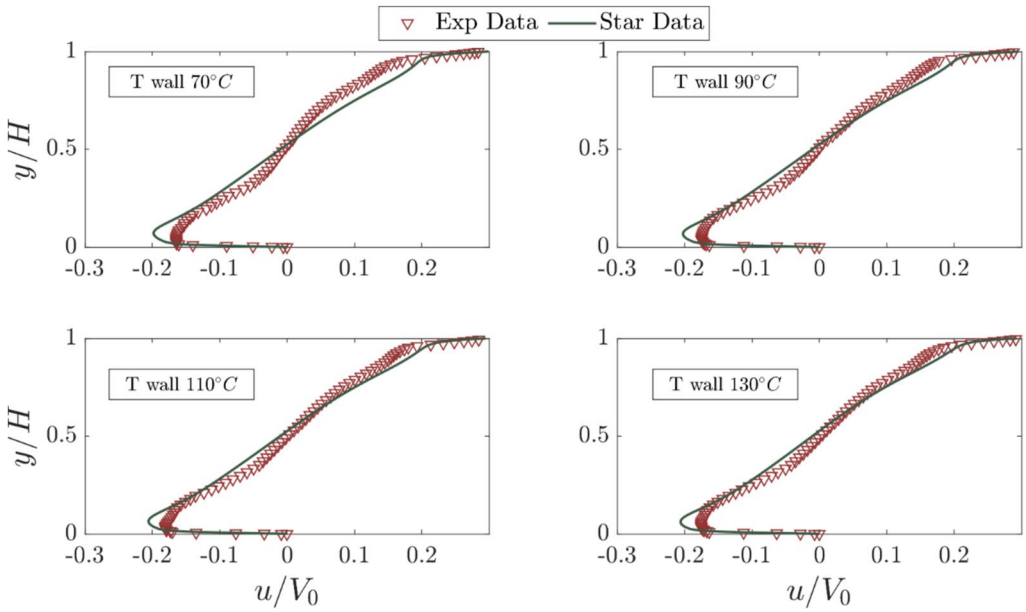

Fig. 5 In green the data obtained with the numerical model. In red the data obtained in the experimental campaign (Allegrini et al. 2013, 2014)

the last 5s of simulation as in the first 15s of the simulation the transient phase was still affecting the results.

Figure 6 shows the velocity fields for the two approaches. The visual comparison reveals minimal differences between the steady-state and unsteady results, suggesting that the flow dynamics in this particular case exhibit quasi-steady behavior. This observation aligns with the expectations for predominantly steady flow in urban canyons under isothermal conditions.

Figure 7 depicts the horizontal (Vx) and vertical (Vz) velocity profiles along the centerline of the canyon. For the URANS simulation, the ±3σ interval is shown as a shaded grey region around the mean values. The low standard deviation indicates that the fluctuations over time are minimal, further reinforcing the idea that the flow can be considered effectively stationary in this scenario. The steady-state results closely match the time-averaged URANS values, confirming the adequacy of the steady-state approach for this case.

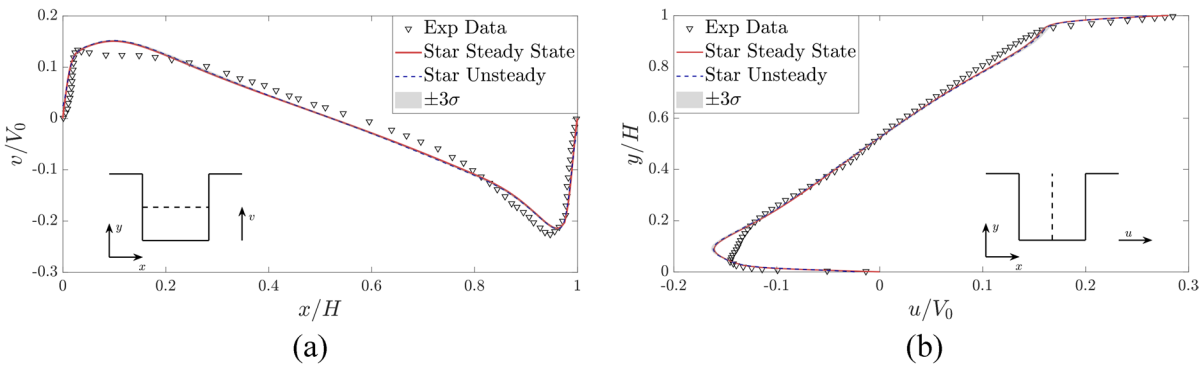

Fig. 6 In black the velocity measured in the experimental campaign. In red the results obtain with the numerical model for BS4 in steady state and in blue the results with the same numerical setup but in unsteady condition

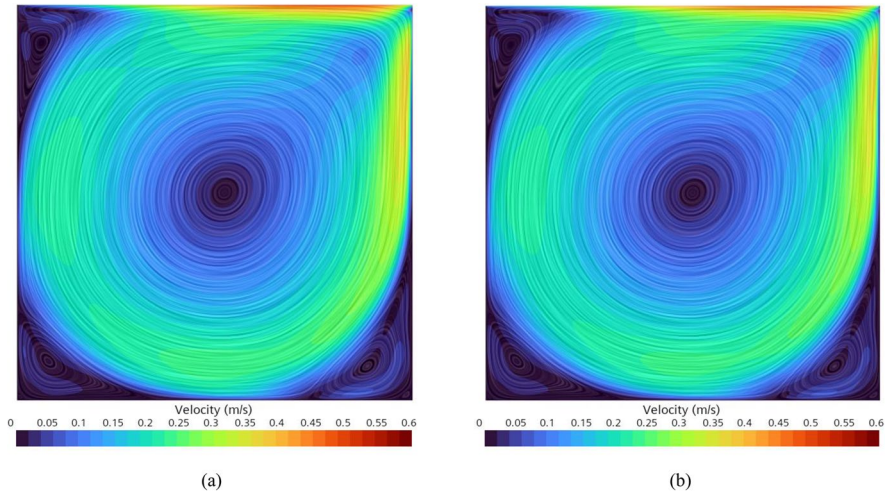

Fig. 7 on the left the velocity field of the steady state case meanwhile on the right the velocity field of the unsteady case after the transient phase is completed

Overall, the comparison between RANS and URANS models reveals negligible differences in both the velocity field and the centerline velocity profiles. This suggests that, for the specific flow conditions analyzed here, the steady-state model is sufficient to capture the essential flow characteristics, with the unsteady model offering no significant additional insights.

Limits of the study While the 2D simulations employed in this study provide a valuable and computationally efficient means of analysing flow and thermal phenomena within urban street canyons, it is important to acknowledge the inherent limitations of this approach. Specifically, 2D simulations cannot fully capture the three-dimensional nature of turbulence, which is a critical aspect of flow dynamics in real-world scenarios. As a result, certain complex turbulent interactions and vertical exchange processes may not be accurately represented. We recognize that this simplification could lead to discrepancies between the simulation results and actual 3D flow behaviour, particularly in areas where turbulence plays a significant role. Despite these limitations, the agreement with experimental data suggests that the key flow features relevant to our study are well-captured, making the findings useful for the intended analysis. Future work will consider 3D simulations to address these limitations and further enhance the model's accuracy.

Climate data

The local climate input data are the reference wind direction DirV [0°N-clockwise] and velocity U_{ref} [m·s^{-1}], the air temperature $T_{C,air}$ [°C], the direct normal solar irradiation I_b [W·m^{-2}] and the diffuse solar radiation I_d [W·m^{-2}]. In this work, weather data has been collected from the weather station of the Living Lab of Polytechnic of Turin, located at 32m from the ground (https://smartgreenbuilding.polito.it). The climate data used is referred to the year 2022, selected as it has no missing or null values; the timespan is a quarter of an hour. To consider only the component incident to the buildings' façade in the canyon, the incident solar radiation I_{inc} [W·m^{-2}] has been calculated as Eq. (2), considering only the hours of the day in which the building façade is irradiated by the sun, depending on the height of the sun from the ground (β>0):

$$I_{inc} = \left(I_b \bullet \cos\beta\right) + \left(SVF \bullet I_d\right) \quad (2)$$

where: β [°] is the incident angle of the sun on the building façade in each hour of the day and Sky View Factor (SFV) is the portion of the sky visible for each specific point on building's facade.

To simulate the non-isothermal condition in the street urban canyon, the delta of the air temperature (ΔT) in the canyon is determined, as according to Eq. (3), by considering the difference between the temperatures of the air layers adjacent to the façade not exposed to solar radiation (cold façade) and the one exposed

to the incident radiation I_{inc} (warm façade). The first corresponds to the external air temperature $T_{K,air}$ [K], while the second to the sol-air temperature $T_{K,s\text{-}a}$ [K].

$$\Delta T_{canyon} = \left| T_{K,s-a} - T_{K,air} \right| \tag{3}$$

$T_{K,s\text{-}a}$ is a fictitious temperature that considers the conductive and convective heat exchanges contributions affecting the external surface of a building with the external air and the solar radiation received by the building facade (Lenin et al., 2022). Therefore, - the absorption factor of the building enevelope α [-], the convective exchange capacity h_e [W·m^{-2}·K^{-1}] and the incident solar radiation I_{inc} [W·m^{-2}] are used in the definition of the sol-air temperature. Its complete definition is expressed by the three-components equation Eq. (4.1):

$$T_{K,s-a} = T_{K,air} + \left(\alpha \bullet \frac{I_{inc}}{h_e} \right) + \left(\frac{\varepsilon \bullet \sigma \bullet \left(T_{K,sky}^4 - T_{K,air}^4 \right)}{h_e} \right) \tag{4.1}$$

where: $T_{K,air}$ is air temperature, α is the absorption factor, h_e the coefficient of external adduction for horizontal heat flow, I_{inc} the incident solar radiation , ε is the emissivity of the surface (0.9 W·m^{-2}), σ is the Stefan-Boltzmann constant (5.67·10^{-8} W·m^{-2}·K^{-4}), and $T_{K,sky}$ is apparent temperature of the sky.

Reference is made at the he UNI EN ISO 6946:2008 and UNI 10349-1:2016. In this paper, the absorption factor α is intended for walls with medium color (0.6), and the coefficient of external adduction h_e for horizontal heat flow is applied according to wind velocity (i.e., 25 W·m^{-2}·K^{-1} for 4-5 m/s and 12.5 W·m^{-2}·K^{-1} for 1 m/s).

The two-components equation Eq. (4.2) is a simplified version of the previous equation:

$$T_{K,s-a} = T_{K,air} + \alpha \bullet \frac{I_{inc}}{h_e} \tag{4.2}$$

The example of the sol-air temperature reported in Table 2 starts from monthly air temperatures, water vapor pressure and incident solar radiation of the case-study and it is determined according to both the three-components equation (Ts-a,3) and the two-components equation (Ts-a,2); then the relative error [%] is calculated. For each month, the relative error is calculated as the discrepancy between the two results: in all months it represents less than 10%. Due to that, it is assumed the possibility to use the simplified two-component equation (4.2), for case-studies in which detailed information about sky conditions is not available.

2D CFD simulations with STARCCM

The cases shown in Fig. 8 have been implemented in the Star CCM+ environment following methodology exposed previously. The CFD simulations aimed to investigate the velocity field within the canyon, weighting the different contributions provided by the cross wind and thermal buoyancy. This last has been generated by an imposed ΔT between the facades of the two buildings in the canyon.

The simulations are organized considering three different aspect ratios representing: narrow, medium and large urban canyon. In addition, to highlight separately the contribution of the two natural phenomena

Table 2 The sol-air temperature according to Eqs. (4.1) and (4.2)

			Months											
			1	2	3	4	5	6	7	8	9	10	11	12
	T_{air}	[°C]	1.3	3.2	8.4	12.0	18.1	22.2	23.7	22.7	19.2	12.4	6.9	2.7
	e	[Pa]	558	618	888	934	1355	1616	1584	2003	1659	1180	925	654
	I_{inc}	[Wh·m^{-2}]	1278	2139	3250	4444	5472	6333	6667	5611	4056	2500	1333	1083
3 components Eq. (4.1)	$T_{s\text{-}a,3}$	[°C]	6.73	10.29	17.04	22.54	29.60	34.92	37.51	34.69	29.14	19.76	11.88	7.56
2 components Eq. (4.2)	$T_{s\text{-}a,2}$	[°C]	5.38	8.72	15.27	20.03	26.90	31.82	33.94	32.09	26.84	18.00	10.71	6.33
	Relative error		-9%	-4%	-1%	1%	1%	1%	1%	1%	1%	0%	-3%	-8%

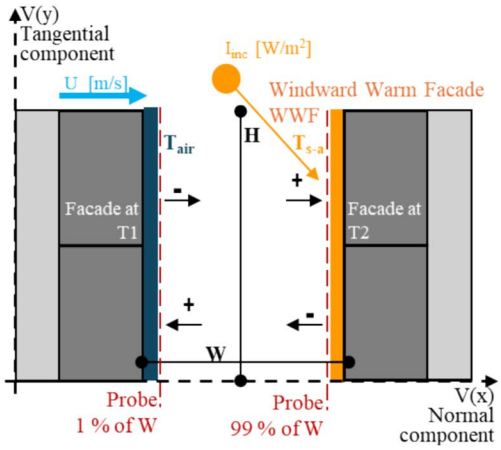

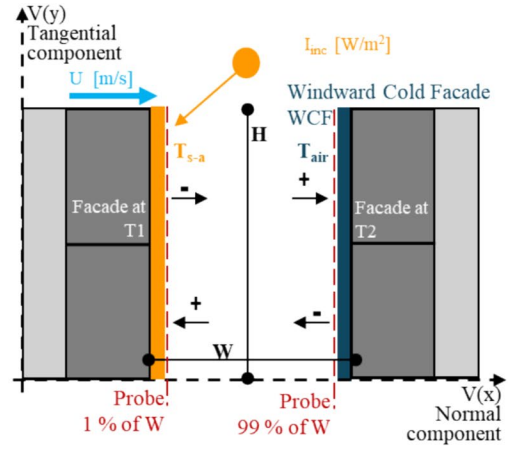

Fig. 8 Cross section of the urban canyon (aspect ratio H/W), considering wind-driven velocity (U) and thermal buoyancy ($\Delta T = T_{air}-T_{s-a}$) due to incident solar irradiation (I_{inc}) and concurrent effects on the windward warm façade (left scheme) and disjointed effects on the windward cold facade (right scheme). Tangential V(y) and normal V(x) components of the wind profile at probes located at 1% and 99% of the W dimension, generate entering (+ arrow) and outgoing (- arrow) air flows through facades

in the creation of vortices structures and velocity field, the wind-driven and the buoyancy effect are evaluated considering extreme local climate condition, with respectively:

- the hourly maximum value of wind speed (*U max*)
- the hourly maximum values of incident solar radiation (I_{inc} *max*)

For each examined aspect ratios, the extreme climatic conditions *U max* and I_{inc} *max* are determined separately in three different bimestrial periods, representative of the winter, summer, and mid-season. Then, each simulation with define condition of urban canyon geometry and climate condition has been evaluated in two opposite scenarios:

- the WWF scenario, where the windward building façade is also exposed to solar radiation (warm façade), and so the two effects are concurrent (Fig. 8, left scheme).
- the WCF scenario, where the windward building façade is not exposed to solar radiation (cold façade), and so the two effects occur on opposite facades in the canyon (Fig. 8, right scheme).

The aim is to describe how concurrent or disjoined effects can impact on the vortical presence and structure in the domain field, also affecting the wind velocity field. The simulation campaign foresees 36 simulations, as schematized in Table 3.

In order to evaluate the velocity law along the canyon, the model has foreseen two probes located near the two facades, recording the whole velocity profile at different heights from the ground. In detail: the 1% and the 99% probes refer respectively to the leeward and windward façades, calculated as the percentage of the canyon dimension (W) (Fig. 8) which varies in relation to the 3 proposed aspect ratio cases. For each point on the probe's axis, both the tangential and normal component of wind velocity has been obtained.

Table 3 Criteria for CFD simulations campaign

Aspect ratio	Effect	Period	Scenario
Narrow Canyon (NC)	Wind-driven (U max)	Winter (WIN)	Windward Cold Façade (WCF)
Medium Canyon (MC)	Buoyancy (I_{inc} max)	Mid-season (MID)	Windward Warm Façade (WWF)
Large Canyon (LC)		Summer (SUM)	

Polynomial function

The velocity profiles obtained through the CFD simulations have been interpolated within the *Matlab* environment using a fifth-grade polynomial function, as Eq. (5). The wind velocity f(x) in the urban canyon was evaluated on the façade of the building as a function of its height x. This function depends on canyon dimension, climate data and vortical structure, considering the 36 conditions mentioned in Table 1. Then for each quota x, the wind velocity is represented by Eq. (5):

$$f(x) = p_1x^5 + p_2x^4 + p_3x^3 + p_4x^2 + p_5x + p_6 \quad (5)$$

The coefficients obtained for each configuration under investigation have been used for the calculation of the wind velocity as it is one main variable influencing the ach.

Ventilation assessment at building level

Lumped parameter model

The lumped-parameter is a zero-dimensional model in which the building tridimensional structure is schematized as a simple network describing the motion of the air flow inside the building through a finite number of interconnected zones. Referring to a network model based on the theory of oriented graphs, the relationships between the different elements of the network system (nodes, links) can be described mathematically. The building is represented as a network of nodes (zones) connected by links, which describe the displacement of the air flow in space. The lumped parameters model is based on the following assumptions:

- in each zone (node) the physical pressure, temperature, and air density conditions are constant throughout the relevant volume of the zone;
- the air flow between the different zones occurs through the openings' leakages, represented as one-dimensional connections (links) between the different volumes of the building (i.e., points of the network);
- the air is supposed to be incompressible, and its motion, caused by the difference in pressure between zones, is due solely to natural causes. These are the surface pressure generated by the incident wind on the external envelope of the building (wind effect) and the spatial gradients of temperature that determine convective actions (stack effect).

In this work, a three-zone air flow model is studied, as schematized in Fig. 9, considering two heated zones, representing the apartments, one no-heated zone, representing the building shaft and the outdoor environmental conditions around the building's facades. The air flows through openings' leakages (Fig. 9, in pink) that contribute to the pressure variation between two zones due to the combined effect of incident wind and thermal buoyancy.

In each zone (node) are associated constant condition of physical pressure P [Pa], temperature T [K], air density ρ [kg·m^{-3}] and height z [m a.s.l.]. For external nodes (Fig. 9, green points) pressures are known, for internal nodes in the barycenter of the zone's volume (Fig. 9, red points) pressure is the unknown variable. Inside each zone, nodes at leakage level (Fig. 9, blue points) are positioned in the barycenter of the opening, and the local pressure is determined in relation to the pressure of the reference zone in the barycenter of the zone's volume. At each link are associated the pressure variation ΔP between two nodes, the air flow $\dot{m}$ [kg·s^{-1}] and a direction. In this work, positive fluxes are the ones outgoing from a node.

Input data

The main input data for the 3-zones airflow model referring to the building scale are:

- building geometry and dimension distinguish the volume of the heated zones and the shaft;
- characteristics of the openings: two types are considered (window, door) with predefined dimensions and area A_{op}, the height z_{op} from the ground level is calculated in the barycenter of each opening;
- characteristics of the leakage whose height z_{leak} coincides with z_{op} and other important parameters that influence the type of air motion, described in the below paragraph.

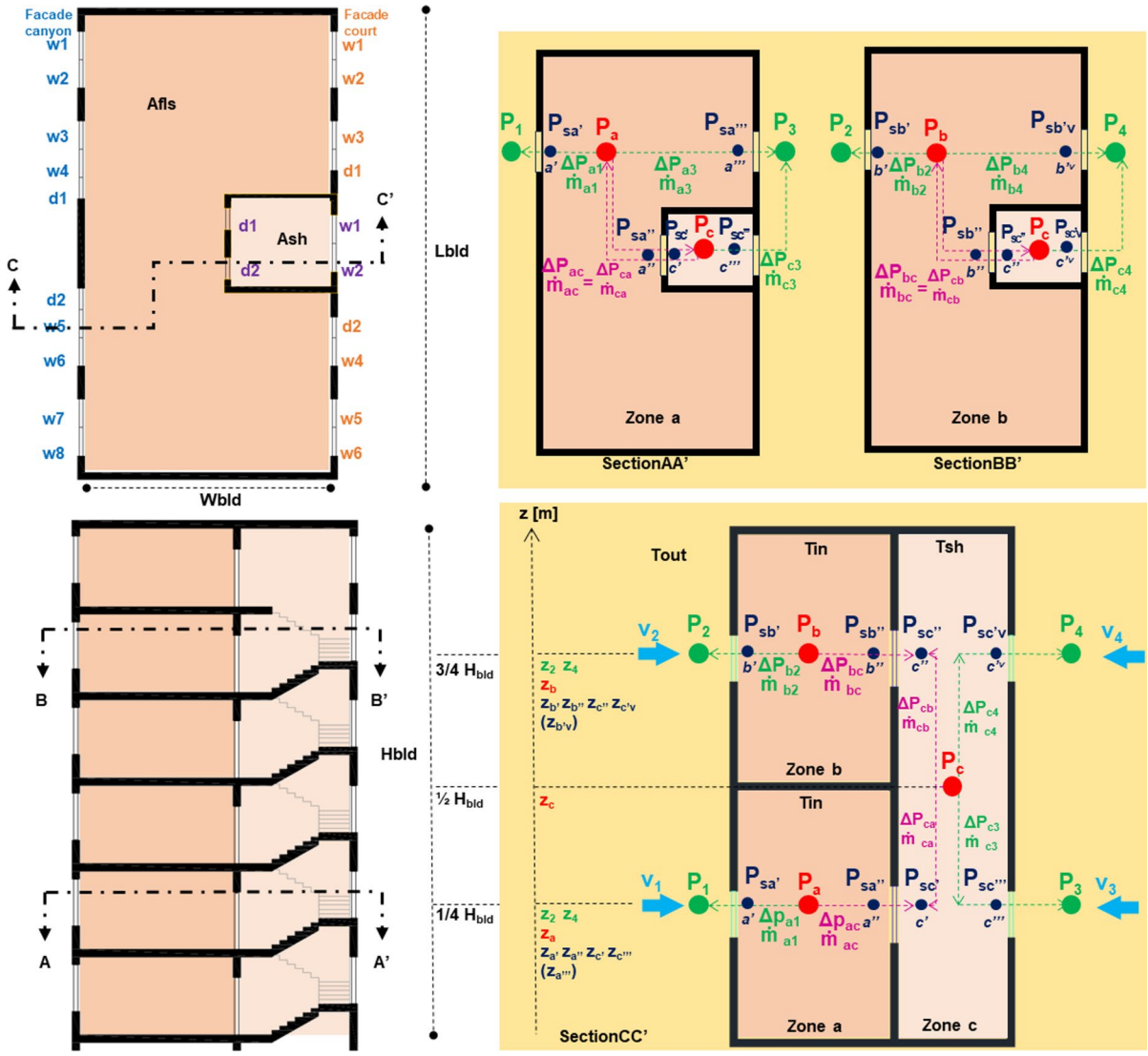

Fig. 9 Scheme of the three-zone air flow model

Table 4 Leakages' characteristics according to opening type and tightness characteristic

Opening Type	Discharge coefficient	Typical Leakage area	Tightness description	Opening area	Equivalent leakage area	Ref.
	Cd [-]	$A_{t,leak}$ [cm^2/m^2]	-	A_{op} [m^2]	$A_{e,leak}$ [m^2]	
Window	0.65	12	Very Loose	(1.2x1.8)	0.0026	(Mckeen & Liao, 2019)
Door	0.65	6	Loose	(0.9x2.2)	0.0012	"

Leakages' characteristics A typical leakage area $A_{t,leak}$ is associated to each opening type, according to the air tightness of the component, reported in Table 4. It is used to calculate the equivalent leakage area $A_{e,leak}$ as shown in Eq.(6).

$$A_{e,leak}\left[m^2\right] = A_{t,leak} \bullet A_{op} \tag{6}$$

Then, the discharged coefficient *Cd* for cracks in walls and floors has a range between 0.6 to 0.7: in this work Cd is fixed at 0.65. For each opening type, the flow coefficient *K* can be calculated according to Eq. (7); it is intended as the value of the flow rate induced by a unitary pressure difference.

$$K_{leak} = Cd \cdot A_{e,leak} * \left(2 * \rho_{in}\right)^{1/2} \tag{7}$$

The parameters *n* is the flow exponent that describe the type of motion of the fluid, depending on the dimension and characteristics of the cracks and theoretically varies between 0.5≤n≤1, from a fully turbulent flow to a laminar one (Allard & Herrlin, 1989). Table 5 reports some of the common values used in scientific literature to describe the airflow rate through different types of leakages.

Referring to the environmental climate condition, the main input data are the wind velocity and the outdoor temperature, that respectively impact on the wind-driven and thermal buoyancy effects.

The outdoor air temperature $T_{C,out}$ corresponds to the hourly value of $T_{C,air}$ from the reference weather station. According to the local climate scenario, the indoor air temperature $T_{C,in}$ of the heated zones inside the building refer to a fixed set point temperature typical of heating and cooling seasons, respectively 20°C and 26°C. As the shaft is a no-heated zone, its temperature is calculated according to Eq. (8):

$$T_{C,sh}\left[^{\circ}C\right] = T_{C,out} + b_{tr,u} \cdot \left(T_{C,in} - T_{C,out}\right) \tag{8}$$

where: $b_{tr,u}$ [-] is the correction factor for confined spaces with an external wall and windows, equals to 0.4 (Appendix A, UNI/TS 11300-1: 2014).

The air density [kg·m^{-3}] is each specific zone is determined by Eq. (9), as it is function of the reference density (ρ_{ref} = 1.29 kg·m^{-3}) at the temperature $T_{K,ref}$ (-273.15 K), and the analyzed temperature T_K (out, in or sh):

$$\rho\left[\mathrm{kg} \cdot m^{-3}\right] = \frac{\left(\rho_{ref} \cdot T_{K,ref}\right)}{T_K}. \tag{9}$$

The velocity *v* [m·s^{-1}] refers to the wind incident on the building in the barycenter of each opening both on windward and leeward facades; it varies according to climate conditions, urban obstructions, height, dimensions and number of the openings, and types of leakages.

In this work, two different methods have been used to correct the reference wind velocity U_{ref} [m·s^{-1}] from the meteorological station, considering the characteristics of the urban morphology, orientation and building geometry.

In the first method (Cp method), the pressure coefficients *Cp* have been determined for each external node in Fig. 9, considering its height and position on facades, specifying the windward and leeward ones. As in previous work (Santantonio & Mutani, 2022), the *CpCalc* software has been used considering tabular data, derived from experimental campaigns. A specific field of application is detailed for each input parameter. These are:

- wind incident angle on windward façade (according to wind direction *DirV* and the azimuth of the building),
- wind profile exponent (roughness parameter *υ*) according to the type of environment (0.10 – 0.33 – 0.45),

Table 5 Typical values of the flow coefficient *K* and flow exponent *n* in scientific literature.

	Value	Unit measure	Note	Ref.
K	0.67-3	[kg·s^{-1}·Pa^{-n}]	per m^2 of outer envelope @4Pa	UNI EN 15242:2008
n	0.5≤n≤1	[-]	-	(Feustel, 2013)
	0.667		-	UNI EN 15242:2008
	0.65		for array of leaks	(Mckeen & Liao, 2019)
	0.5		for large opening	(Dols & Polidoro, 2020)
	0.65		for small crack-opening	
	0.6≤n≤0.8		-	(Mun et al., 2021)

- Plan Area Density *PAD* (0 – 12.5 – 25 – 50),
- Surrounding building Height *SbH* (0 – 0.7 – 0.93 – 1),
- building orientation, geometry, Frontal Area Ratio *FAR* (0.5 – 4) and Side Area Ratio *SAR* (0.5 – 2) and
- coordinates describing the position of openings on windward and leeward facades' area.

The second method (CFD method) uses the output results of CFD simulations for given climate conditions, canyon geometry and vortical structure. The wind velocity at a specific height of an opening is obtained by the polynomial function in Eq. (5) for the conditions corresponding to the case study. So, for all external nodes in Fig. 9, the wind velocity obtained is derived directly from the CFD simulation.

Other input data are the gravity g [m·s^{-2}] and the reference atmospheric pressure $P_{atm,ref}$ at 0 m asl, equals to 101325 Pa and the altitude *alt* in [m asl] of an examined case study.

Mass and energy conservation

Referring to the fundamental equations of mass and energy conservation, in each node in the network must exist a mass flow balance driven by a delta pressure and the algebraic sum of all the air flows is zero, according to Eq. (10) or written in vector form as Eq. (10.1):

$$f(\Delta P) = \sum_{L=1}^{L_i} \pm \dot{m}_i \tag{10}$$

where: i a generic node and L_i, the number of links that flow into the node, $\dot{m}$ [kg·s^{-1}] the mass air flow rate entering (-) or outgoing (+) from the node through each link L.

$$f(\Delta P) = 0 \tag{10.1}$$

For the three-zone air flow model in Fig. 9, a system of 3 equations can be written Eq. (11):

$$\begin{cases} \dot{m}_{a1} + \dot{m}_{a3} + \dot{m}_{ac} = 0 \\ \dot{m}_{b2} + \dot{m}_{b4} + \dot{m}_{bc} = 0 \\ \dot{m}_{ca} + \dot{m}_{cb} + \dot{m}_{c3} + \dot{m}_{c4} = 0 \end{cases} \tag{11}$$

For each link, the mass flow rate $\dot{m}$ [kg·s^{-1}] is described as a function of the pressure difference between two nodes, according to Eq. (12.1), considering the characteristic of the opening's leakage (dimension and typology). Here, the exemplifying nodes a and c (Fig. 9) are considered:

$$\dot{m}_{ac} = C_d \bullet A_{e,leak} \bullet \rho \cdot \sqrt{\frac{2\Delta P_{ac}}{\rho}} \tag{12.1}$$

where: Cd is the relative discharge coefficient [-], ρ the air density [kg·m^{-3}], ΔP the pressure difference and $A_{e,leak}$ is the effective flow area of the cracks [m^2] between two zones (Equivalent leakage area in Eq. 6).

In most cases, a general law can be used, defined as Eq. (12.2); the mass flow rate $\dot{m}$ [kg·s^{-1}] is described as a function of the pressure difference between two, considering the characteristic of the leakages (K, n):

$$\dot{m}_{ac} = K_{ac} \cdot \left(\Delta P_{ac}\right)^n \tag{12.2}$$

where: K is the flow coefficient [kg·s^{-1}·Pa^{-n}] and n is the flow exponent [-], calculated as Eq. (7) and described in Table 3.

Pressure variation

The air flow within two generic nodes (i,j) is governed by Bernoulli's equation Eq. (13):

$$\frac{1}{2}\rho v_i^2 + P_i + g\rho z_i = \frac{1}{2}\rho v_j^2 + P_j + g\rho z_j + \Delta P xy \tag{13}$$

where: $\underline{\Delta P_{xy}}$ is the concentrated pressure drop due to the presence of the leakage. In determining the total pressure condition P, in each node both kinetic and potential pressure contributions are considered.

External nodes (P at nodes 1,2,3,4) The dynamic pressure p_{dyn} at each external node *i (with i from 1 to 4)* is generated by the effect of the natural wind

on both the windward and leeward façade. It can be calculated according to Eq. (14.1) in application to the *Cp-method* and Eq. (14.2), in application to the *CFD-method*:

$$p_{dyn_i} = \frac{1}{2}\rho_i \cdot Cp_i \cdot U_{ref}^2 \tag{14.1}$$

where: U_{ref} is the undisturbed wind velocity [m·s^{-1}] from the reference weather station, ρ [kg·m^{-3}] is the outdoor air density, and Cp [-] is the experimental pressure coefficient at leakage's position calculated with the tool *CpCalc* tool, as a function of the building dimensions and orientation, wind profile exponent and class of PAD.

$$p_{dyn_i} = \frac{1}{2}\rho_i \cdot \left(v_i^2\right) \tag{14.2}$$

where: v [m·s^{-1}] is the wind velocity at leakage's position inside the canyon, calculated from the CFD simulation, considering the effect of windward (+) and leeward (-) dynamic pressure on the façade, and ρ [kg·m^{-3}] is the outdoor air density.

The pressure p_i at each external node i is determined as Eq. (15) adjusting the reference atmospheric pressure P_{atmref}, considering the local altitude *alt* [m asl] and the height of each node z_i :

$$p_i = p_{atm_{ref}} \bullet 0.9877^{\frac{(alt+zi)}{100}} \tag{15}$$

The potential pressure p_{pot} at each external node i is determined as Eq. (16):

$$p_{pot_i} = \rho \cdot g \cdot z_i \tag{16}$$

where: g [m·s^{-2}] is the gravity, ρ [kg·m^{-3}] is the outdoor air density and z_i the height of each node.

As in the 3-zones airflow model the outdoor boundary conditions are known, in each external node i the total pressure P_i is defined according to Eq. (17):

$$P_i = p_{dyni} + p_i + p_{poti} \tag{17}$$

Internal nodes (P at nodes a,b,c) In each internal node j (red nodes in Fig. 9*)* the boundary condition known are the indoor air density ρ_j [kg·m^{-3}], and the height of each node z_j [m]. It is not possible to directly determine the total pressure contribution P_j, according to Eq. (17), since the indoor dynamic contributions is not known, and only the potential contribution can be calculated, according to Eq. (16).

An iterative calculation will be used to determine the output value of P_j : the initial values p_{j0} are needed and they are calculated as the sum of the internal pressure contributions Eq. (18), considering the following hypothesis:

$$p_{j0} = p_j + p_{dynj} \tag{18}$$

– dynamic pressure $p_{dyn\ j}$ at each internal node j is calculated according to Eq. (19), as it is generated by the velocity of indoor air v_{int} that is assumed to be the same for all zones,

$$p_{dyn_j} = \frac{1}{2}\rho_j \cdot \left(v_{int}^2\right) \tag{19}$$

where: v_{int} [m·s^{-1}] is the wind velocity at leakage's position inside the zones (v_{int} =3 m·s^{-1}).

In this work, the stack-effect is considered separately inside the specific volume of each internal zone, and it considers the variation of nodes' height between different nodes in the same zone that directly affects the contribution of the potential pressure to the total pressure. Assuming a constant velocity of the air flow and no pressure drop within each zone, it is possible to apply the Bernoulli's equation to each couple of nodes, excluding the kinetic contribution in determining the pressures at the nodes. The relationship described by Eq. (20) is applied to each node j at the barycenter of the zone's volume (red points in Fig. 9) and each correspondent node j^n at leakages' level (blue points in Fig. 9) for all the n openings in the same zone.

$$p_j + p_{pot_j} = p_{j_n} + p_{pot_{jn}} \quad \rightarrow p_{jn} = p_j + \rho_j g\left(z_j - z_{jn}\right) \tag{20}$$

In the presented model, the stack-effect occurs only in the shaft (zone c), where the height z_c in the barycenter of the zone's volume is different from the height of the four nodes at leakage level ($z_c > z_{c'}$, $z_c > z_{c''}$, $z_c < z_{c''}$ and $z_c < z_{c'v}$). Applying Eq. (20) between node c and each of the four nodes at leakage, it is possible to assign the following relations:

$$p_{c\prime} = p_c + \rho_c g\left(z_c - z_{c'}\right) \text{ at leakage } c^{'} \tag{20.1}$$

$$p_{c\prime\prime} = p_c + \rho_c g\left(z_c - z_{c''}\right) \text{ at leakage } c^{\varepsilon} \tag{20.2}$$

$$p_{c'''} = p_c + \rho_c g\left(z_c - z_{c'''}\right) \text{ at leakage } c^{\varepsilon'} \tag{20.3}$$

$$p_{c'v} = p_c + \rho_c g\left(z_c - z_{c'v}\right) \text{at leakage } c^{'v} \tag{20.4}$$

In both zones *a* and *b*, three nodes at leakage level exist (blue points in Fig. 9). Since their height corresponds to the height of the node in the barycenter of the zone's volume, (z_a=$z_{a'}$=$z_{a''}$=$z_{a'''}$) and (z_b=$z_{b'}$=$z_{b''}$=$z_{b'v}$), and the local air density is the same within the volume of each zone, no stack-effects occur in these zones, and for each node at leakage, it is possible to affirm that: $p_a = p_{a'} = p_{a''} = p_{a'''}$, in zone *a,* and $p_b = p_{b'} = p_{b''} = p_{b'v}$ in zone *b*.

For zone *a* and *b*, there is no difference in calculating each of the three pressure contributions at leakage level j_n or in the barycenter node *j*. Due to the stack effect in the shaft, it is necessary to consider the following relation Eq. (21), for each of the four (n) existing leakages:

$$P_{c_n} = p_{dyn_c} + p_c + p_c g_c\left(z_c - z_{c_n}\right) + p_{pot_{c_n}} \tag{21}$$

where it is possible to rewrite $p_{dyn_c} + p_c = p_{c_0}$, according to Eq. (18) and rename $\rho_c g\left(z_c - z_{c_n}\right) = p_{stk_c n}$. The system of equations (11) can be re-written as Eq. (22a,b,c) that correspond to function F of the iterative calculation; reference is made to the nodes at leakages j_n.

$$\begin{cases} K_{a'1}\left(p_{a0} + p_{pota} - P_1\right)^n + K_{a'''3}\left(p_{a0} + p_{pota} - P_3\right)^n + K_{a''c'}\left(p_{a0} + p_{pota} - p_{c0} - p_{potc'} - p_{stkc'}\right)^n = 0 \\ K_{b'2}\left(p_{b0} + p_{potb} - P_2\right)^n + K_{biv4}\left(P_{b0} + p_{potb} - P_4\right)^n + K_{b''c''}\left(p_{b0} + p_{potb} - p_{c0} - p_{potc''} - p_{stkc''}\right)^n = 0 \\ K_{c'a''}\left(p_{c0} + p_{potc'} + p_{stkc'} - p_a - p_{pota}\right)^n + K_{c''b''}\left(p_{c0} + p_{potc''} + p_{stkc''} - p_b - p_{potb}\right)^n + \dots \\ K_{c'''3}\left(p_{c0} + p_{potc'''} + p_{stkc'''} - P_3\right)^n + K_{c'v4}\left(p_{c0} + p_{potc'v} + p_{stkc'v} - P_4\right)^n = 0 \end{cases} \tag{22a,b,c}$$

Then, the initial value p_{j0} of the iterative calculation, is assumed to be in a range whose lower (*low*) and upper (*upp*) limits are defined according to Eq. (23.1) and Eq. (23.2), respectively:

$$p_{j0\_low} = p_j \tag{23.1}$$

$$p_{j0\_upp} = p_j + p_{dynj} \tag{23.2}$$

Iterative procedure

Equations 22a,b,c cannot be solved analytically; therefore, numerical methods were used. To find the solution of Eq. 22a,b,c, numerical methods find the zeros of the functions: the solutions P for which f(P)=0.

In this work, Matlab software was chosen to automatize the iteration process to find the numerical solution using *fsolve* function. *Fsolve* provides several algorithms for solving non-linear equations with the Newton-Raphson method; among them, the *trust-region* (*tr*) has been used. *Fsolve* requires initial points as vectors; in this work in order to reach the convergence between the 3 solutions of the 3 unknown pressures at internal nodes (P_a, P_b, P_c), the iterative calculation has been set to consider different combination of the 3 initial points (p_{a0}, p_{b0}, p_{c0}) that made up the starting vector. Each of the 3 initial points is defined in a range between the lower limit (p_{j0_low}) and the upper limit (p_{j0_upp}). Within the range of each initial point, ten values were selected at a regular distance, considering the width of each interval; each combination considered the variation of one initial value at a time: a total of 1000 combinations were applied in every iterative calculation. According to the accuracy of these values, the tolerance and stopping criteria applied for the *trust region* algorithm has been defined, as reported in Table 6; this choice is very important to achieve convergence and solve the non-linear system of three equations (Eq. 22a,b,c).

The choice of the correct solution of Eq. (22a,b,c) considers all the possible directions of the outgoing or entering mass flows at nodes of the 3-zone model (positive or negative signs of coefficients *K*), considering the mass conservation of

Table 6 Tolerance and stopping criteria of MatLab fsolve algorithms

Algorithm	Step Tolerance	Function Tolerance	Optimality Tolerance	Max iteration number
tr	$1e^{-06}$	$1e^{-09}$	$1e^{-06}$	400

the links entering in the same node. Then, for each simulation and each combination of the 3 starting points matrix *A* with 126 combinations of the signs of the mass flow rates at each of the ten links ($\dot{m}_{a1}$- $\dot{m}_{a3}$- $\dot{m}_{ac}$ at node a in Eq. (22a), $\dot{m}_{b2}$- $\dot{m}_{b4}$- $\dot{m}_{bc}$ at node b in Eq. (22b, $\dot{m}_{ca}$-$\dot{m}_{cb}$-$\dot{m}_{c3}$-$\dot{m}_{c4}$ at node c in Eq. (22c) was tested and the solution that minimizes the error was chosen:

$$A = \begin{bmatrix} - & - & + & - & - & + & + & + & \dots & (1,10) \\ - & + & - & + & + & - & + & + & \dots & - \\ \dots & \dots & \dots & \dots & \dots & \dots & \dots & \dots & \dots & \dots \\ (126,1) & + & + & + & - & - & - & + & \dots & (126,10) \end{bmatrix}$$

The solution of the system is a triplet of the values of Pa, Pb and Pc which make each of the three equations of the system Eqs. (22a,b,c) closest to zero.

Air changes per hour calculation

The final output data of the presented methodology is the value of the Air Change per Hour (ach) calculated in the three indoor zones of the building: the two zones *a* and *b* heated at T_{in} and the shaft at T_{sh}. Ach is calculated according to Eq. (24),

$$ach\ \left[h^{-1}\right] = \frac{\dot{m}_a \cdot 3600}{\rho_a \bullet Vol_a} \tag{24}$$

where: the main related variables are the air flow rate $\dot{m}$ [kg·s^{-1}], the air density ρ_a [kg·m^{-3}], and the volume vol_a [m^3] of the zone *a;* the same calculation is applied to the other building's zones (*b* and *c*).

The hourly variation of ach is related to the hourly variation of the environmental external condition: outdoor air temperature, and velocity of wind incident.

In this work, the 3-zone air flow model has been applied to a typical building (condominium with six floors in the center of Turin) for different scenarios of outdoor climate conditions, considering the same geometry and leakage characteristics.

Case study

The presented methodology has been applied to a case study in the city of Turin (Italy). The Crocetta district has a regular urban path, representative of the consolidated areas. Previous work (Santantonio & Mutani, 2022) defined it as a homogeneous zone. The main urban parameters to describe urban morphology are the Plan Area Density PAD (0.33), the average height of the building (20m), the typical H/W dimension (0.5) that considers internal courtyard of the block of buildings, and the wind profile exponent (0.4). These are also the main input parameters of the *CpCalc* software, used to assess the Cp values. The district has been chosen due to the presence of regular street canyons with different dimensions, and two prevailing orientations: +30°N (NE-SW) and -60°N

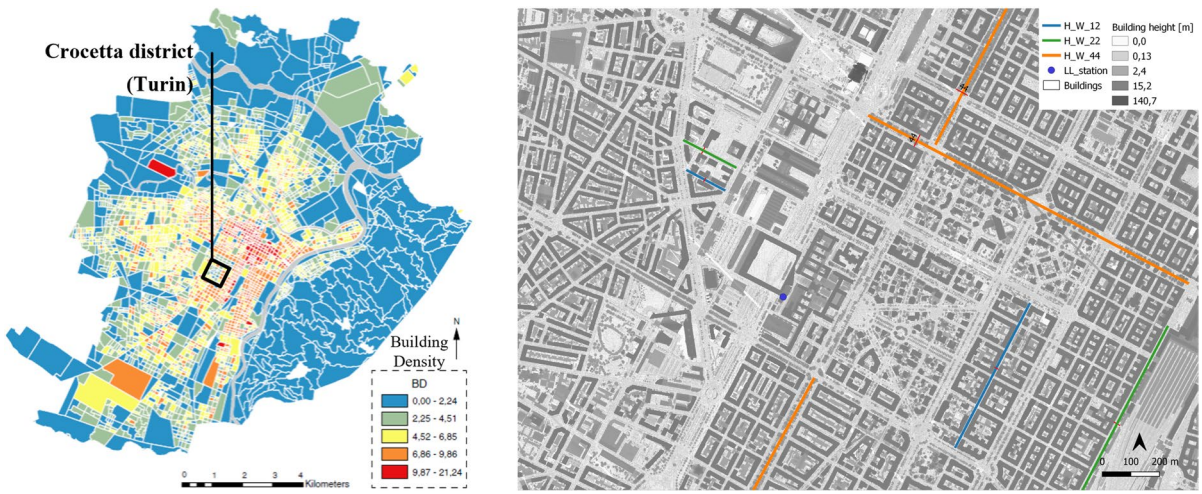

Fig. 10 Localization of the Crocetta district in the city of Turin (on the left) and urban canyons in Crocetta district (on the right) for selected aspect ratio: narrow (in blue), medium (in green) and large (in orange)

Table 7 Aspect ratio examined for the case study

Type of urban canyon	W [m]	H [m]	H/W [-]	NE-SW axis	NW-SE axis
Narrow Canyon (NC)	12	20	1.7	Lamarmora	Vochieri
Medium Canyon (MC)	17	20	1.2	Sacchi	Borsellino
Large Canyon (LC)	46	20	0.4	Vittorio	Duca

Table 8 Extreme climate conditions of hourly wind (Umax) and solar irradiation (Iinc max) in winter (WIN), summer (SUM) and mid-seasons (MID) in the reference year 2022, applied in the CFD analysis

Extreme condition	Period	Date (Year 2022)	U_{ref} [m· s^{-1}]	T_{air} [°C]	T_{s-a} [°C]	I_{inc} [W·m^{-2}]	ΔT [°C]
U max	WIN	02-07 08:00	6.8	9.8	15.0	215.8	5.2
	MID	04-08 17:00	10.7	22.6	32.2	401.9	9.6
	SUM	06-28 14:00	8.6	20.5	22.1	67.6	1.6
I_{inc} max	WIN	01-11 14:00	2.1	8.5	31.5	957.7	23.0
	MID	04-10 16:00	1.4	16.6	36.9	844.4	20.3
	SUM	06-10 17:00	1.6	31.0	51.1	839.5	20.1

Table 9 Typical climate winter and summer days (hourly data)

Period	U_{ref} [m· s^{-1}]	T_{air} [°C]	T_{s-a} [°C]	I_{inc} [W·m^{-2}]	ΔT [°C]
Winter	0.5	5.6	8.0	96.6	2.4
Summer	0.9	29.2	44.8	648.3	15.6

(NW-SE) that correspond also the prevalent orientation of buildings. In addition, the weather station (LL, Fig. 10) used to collect local climate data is in the same district. In Fig. 10 and Table 7 are shown the 3 types of urban canyon in six streets of Crocetta district simulated in CFD analysis: fixing the height of the canyon to the average building height of the area (20m), 3 aspect ratio H/W are selected, according to the width of the street. Narrow urban canyons (NC) are representative of the internal streets in regular building blocks, while the medium (MC) and large (LC) canyons insist on the perimetral axis of blocks.

The extreme climate data conditions used in the CFD simulations are listed in Tables 8 and 9. The local prevailing wind direction (DirV in Fig. 11) is always considered from West-Northwest, (300°N, clockwise). Selected date from the year 2022, considering winter (WIN), mid-season (MID) and summer (SUM), for both extreme climatic conditions of highest hourly wind speed (U max) and hourly incident solar irradiation (I_{inc} max). In the first Umax three cases, the ΔT is low as the crosswind effect is prevalent, while in the second three cases (I_{inc} max), the ΔT is high due to the highest value of the incident solar irradiation on the facade, and the wind velocity is low.

To understand the typical meteorological seasons of the area of interest, two different seasons have been built using the typical meteorological days' approach (Hassan et al., 2021). The meteorological data gathered for Crocetta area has been clustered in three clusters using the k-means algorithm. Once the clusters have been assessed, the minimum and maximum centroids values have been assumed as winter and summer. The results obtained have been presented in Table 7.

According to the typical days, four different scenarios have been identified (Table 10), selecting four different dates from the reference year 2022, to be applied in the three-zones air flow lumped parameter model. It is possible to compare the resulting hourly ach in winter (WIN) and summer (SUM) seasons, considering for both cases low wind speed (no wind) and high wind velocity (windy) conditions.

The case study building for the application of the three zones airflow model is a simplified schematization of building B2, represented in Fig. 11. The main input data regarding the building geometry and opening types are listed in Table 11, while leakages' characteristics are listed in Table 12. The period of construction of the building is before 1918, representative of the typical buildings in the selected area; this influences the tightness description of the openings

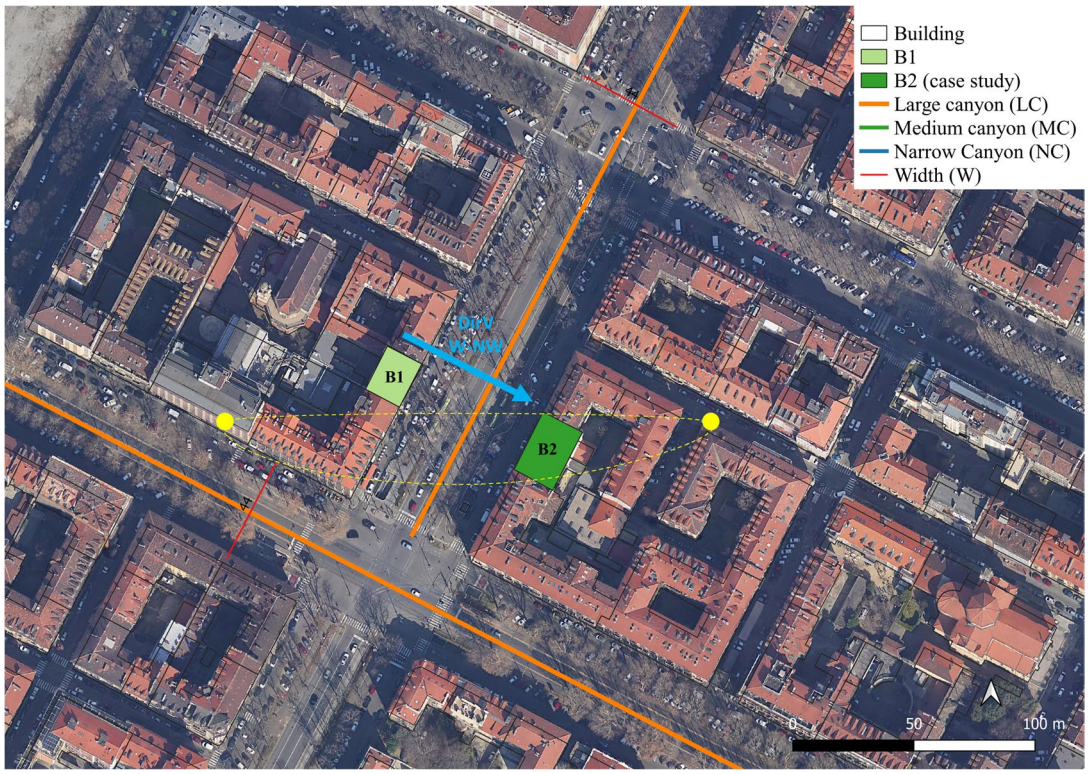

Fig. 11 Localization of the large urban canyon (LC) examined building with NE-SW axis, considering crosswind (DirV) and solar exposures (yellow dot) on the facades of building B1 and B2

Table 10 Climate hourly input data of the 4 scenarios applied in the 3-zone airflow model analysis

Scenario	U_{ref} [m· s^{-1}]	T_{air} [°C]	T_{in} [°C]	T_{s-a} [°C]	I_{inc} [W·m^{-2}]	ΔT [°C]
WIN-windy	5.00	7.0	20	8.53	63.8	1.53
WIN-no wind	1.48	7.0	20	24.19	716.3	17.19
SUM-windy	6.17	28.0	26	33.98	249.2	5.98
SUM-no wind	2.18	28.0	26	42.36	598.3	14.36

Table 11 Description of the case study: building dimension and opening characteristics

		Building geometry		Openings characteristics	
		Zone		Type	
		Heated (a,b)	Shaft (c)	window w	door d
Dimension (LxHxW)	[m]	9x9x7.7	9x18x3.3	1.2x1.8	0.9x2.2
Number	[n]	3 floors	6 floors	8 w (per floor)	2 d (per floor)
Typical leakage area	[cm^2/m^2]	-	-	12	6

Table 12 Description of the case study: height and pressure coefficient of external and internal nodes

		External nodes				Internal nodes			Internal nodes at leakage					
		1	2	3	4	a	b	c	a'	a"-c'	b'	b"-c"	c"'	c'v
Z	[m]	4.5	13.5	4.5	13.5	4.5	13.5	9.0	4.5	4.5	13.5	13.5	4.5	13.5
Cp	[-]	0.005	0.22	-0.03	-0.04	-	-	-	-	-	-	-	-	-

and leakages (Table 11). The building has been chosen to respond to the application field of *CpCalc* software, used to calculate Cp at external nodes (P1, P2, P3 and P4). The openings are located at the lowest and highest parts of the building to observe different conditions of wind incident and to enhance the effect of buoyancy.

Results and discussion

In this section, the results of the two main steps of the work are described. In paragraph 5.1, results of the 2D CFD simulations describe: i) the comparison between the wind velocity profile in front of the leeward façade (probe at 1%), and the windward façade (probe at 99%), ii) the types of vortices that occur in the urban canyons, as a function of their H/W ratio and climate conditions, and iii) the equations that describe the wind velocity as a function of the height (z), considering the disjoined (WCF) or combined (WWF) effect of the cross-wind urban ventilation and non iso-thermal condition.

In paragraph 5.2, results of the 3 zone-air flow model at building scale are presented: i) the air mass flows and the air changes per hour for the four typical winter and summer conditions, in no wind and windy scenarios, ii) the comparison of the results of dynamic pressure, air flow rate, and ach, considering the two applied methodologies (*CpCalc-method* and *CFD-method*).

Results of the 2D CFD simulations

The wind flow profile is affected by the canyon geometry and the boundary conditions (i.e., climate inputs). In the following figures (Figs. 12, 13, 14, 15, 16), the results obtained for the large (LC), medium (MC), and narrow (NC) canyons will be presented, showing separately the contribution of the wind driven effect (Umax) in Figs. 12, 14, 16a, and the thermal gradient effect (Imax) in Figs. 13, 15, 16b, both during the winter and summer season, and for both considering the Windward Cold Facade (WCF) and Windward Warm Façade (WWF) scenarios. Considering the wind driven effect (Umax) in all canyon dimensions, the crosswind contribution is prevalent in determining a central vortex (Fig. 14a-f), and it is not affected by the presence of the irradiated wall; since no relevant differences occur between the WWF and WCF scenario, only results of the WWF scenario are shown.

Figures 12 and 13 show the wind velocity profiles of the steady flow regimeboth in front of the leeward façade (probe at 1%) and the windward façade (probe at 99%).

Figures 14 and 15 show the different contribution of the two extreme effects of the cross wind-driven and thermal gradient in creating the vortex structure in the domain of the urban canyons, as a function of their H/W ratio and climate conditions. Considering the undisturbed wind flow U (blue arrow), the windward façade of building B2 is always on the left of the scheme, and it is analyzed in both the Windward Cold Facade (WCF, in blue) and Windward Warm Façade (WWF, in orange) scenarios.

Regarding the cross wind-driven effect (Umax), in the Large Canyon (LC), a unique vortex occurs, and it has the same symmetrical behavior in all the two seasons analyzed. The same consideration can be done for the other canyons dimensions (MC and NC), but each one has a different intensity of wind velocity.

Regarding the thermal gradient effect, the contribution of the heated wall becomes tangible in the definition of the vortical structures. Oscillating solutions in the domain are obtained when the two effects (crosswind and irradiated wall) occur to the same facade, the flow on warm wall tries to flow upwards due to the buoyancy effect, but it conflicts with the vortex created inside the canyon and by the effect of the external upstreaming wind.

For all the three canyon dimensions, a single vortex is formed only in the case when the windward façade is not irradiated (WCF scenarios) in winter

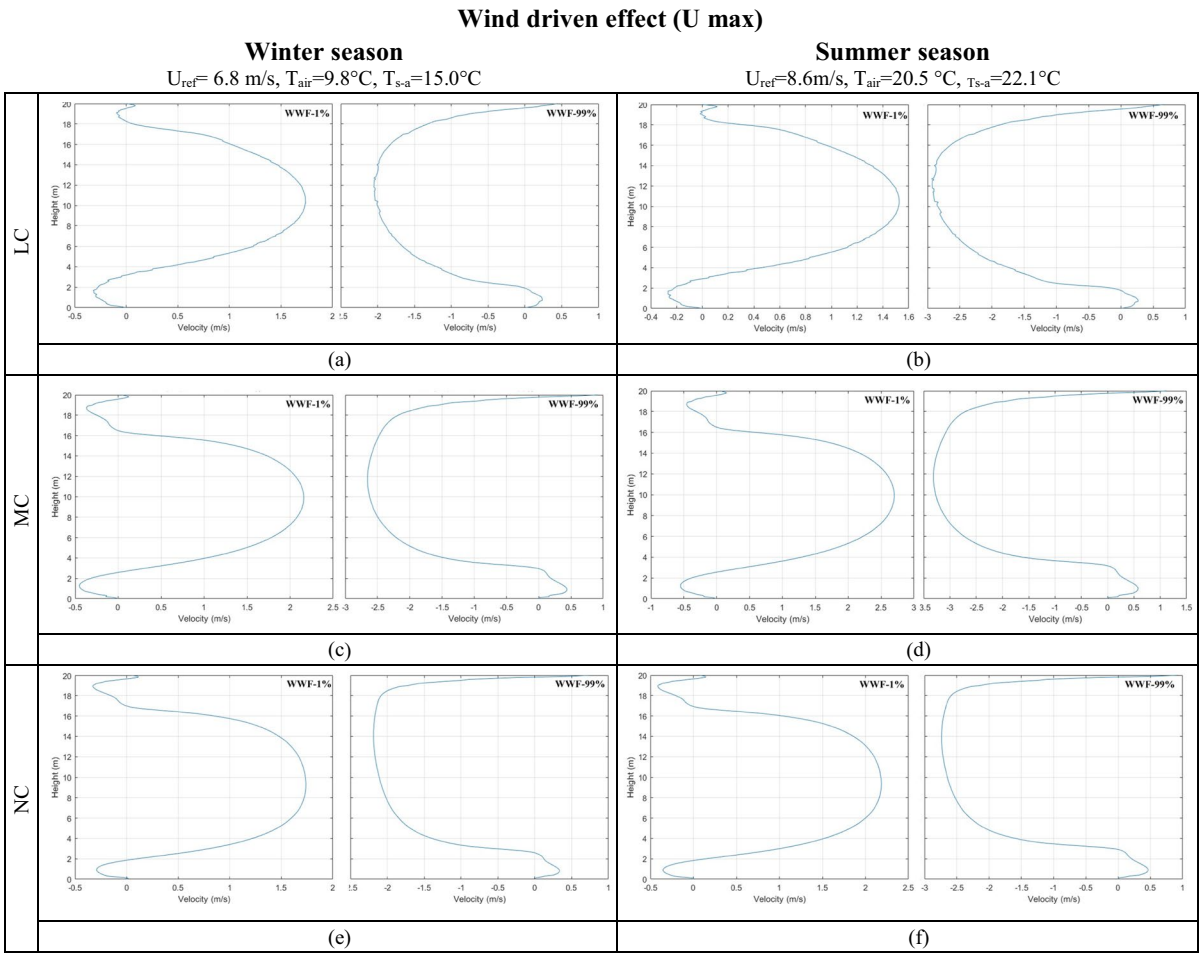

Fig. 12 **a**-**f**. Wind driven (Umax) effect generating wind velocity profiles in large (LC), medium (MC), and narrow (NC) canyons, in front of leeward (1%) and windward (99%) façades, in WWF scenarios, during winter (**a**-**c**-**d**) and summer (**b**-**d**-**f**) seasons

(Fig. 15b-f-l) and summer (Fig. 15d-h-n). Alternatively, when the windward façade is warm (WWF), crosswind and thermal buoyancy effects add up by thickening the mixing layer; one no longer traces a single vortex structure, but several recirculation zones in winter (Fig. 15a-e-i) and summer (Fig. 15c-g-m), and asymmetrical wind velocity profiles are obtained from all the probes in the canyon (Fig. 13a-n).

In all the WCF scenarios in Fig. 15, the vortex is even more symmetrical, and the air increases its velocity, especially near the vertical and horizontal surfaces. the same conditions (I_{inc} max and low U), in case of narrow urban canyon (NC), in each analyzed period,

The graphs in Fig. 16a-b describe the flow field of the crosswind near the windward façade (probe at 99%), in the summer season and WWF scenario (combined effect of wind and buoyancy on the windward façade), considering separately the extreme condition of maximum crosswind Umax (Fig. 14a) and maximum incident irradiation I_{inc} max (Fig. 14b). For each of the three urban canyons (narrow, medium, and large) the plotted curves describe the wind velocity as a function of the height in the canyon. In case of maximum wind Umax, for all canyons the velocity profile is symmetrical with the highest value at half height of the façade. In the large canyon (LC), the wind profile is lower than the ones in the medium and narrow canyons. This last consideration is valid also in Fig. 14b, where the effects of thermal gradient are evident. The warm air flows upwards due to the buoyancy effect, is increased by the presence of the

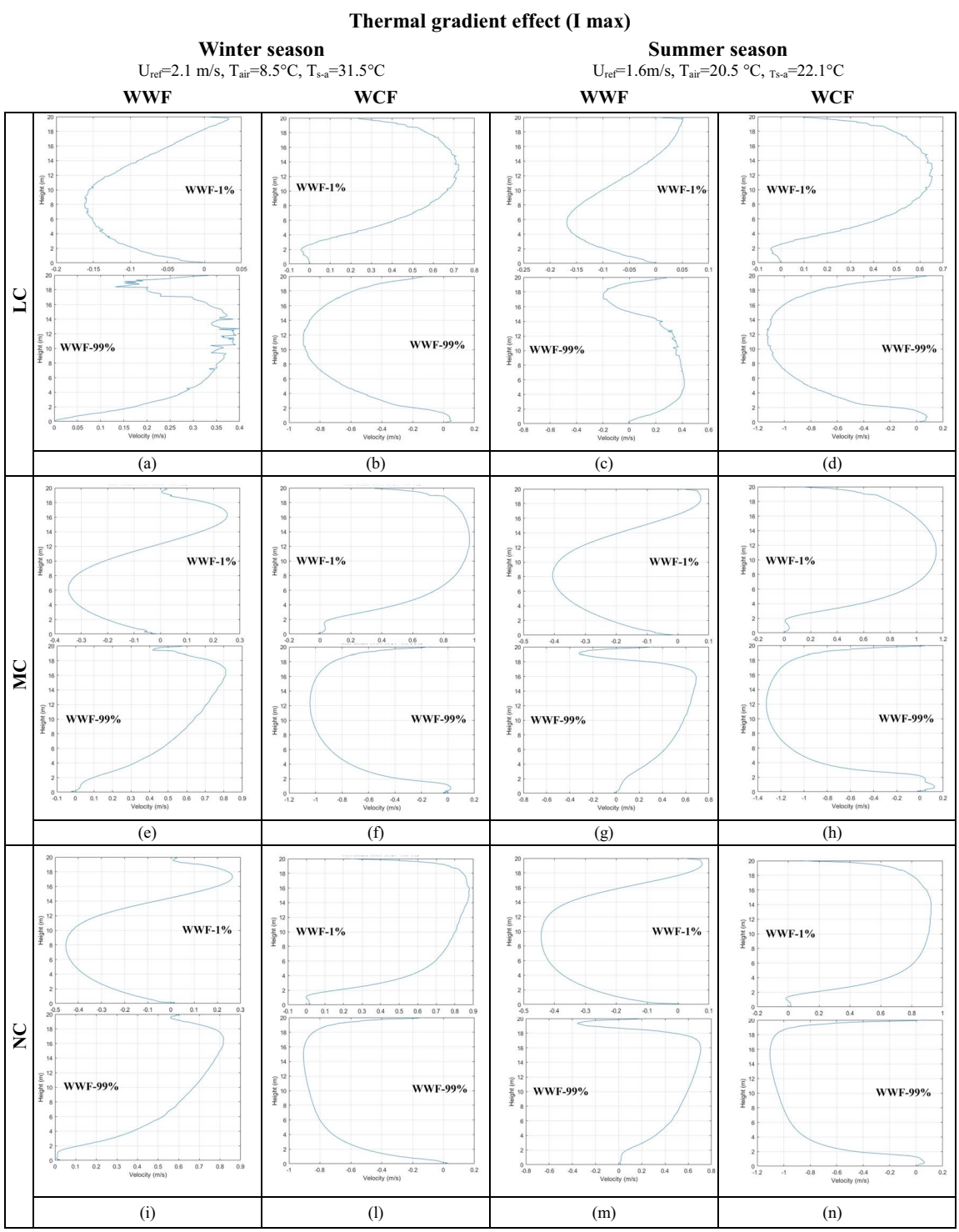

Fig. 13 **a**-**n**. Effect of the extreme condition of thermal gradient (Imax) in generating the wind velocity profiles in large (LC, **a**-**d**), medium (MC, **c**-**h**), and narrow (NC, **i**-**n**) canyons, , in front of the leeward façade (probe at 1%) and the windward façade (probe at 99%), during the winter (**a**-**b**-**e**-**f**-**i**-**l**) and summer (**c**-**d**-**g**-**h**-**m**-**n**) seasons, and Windward Warm Facade (WWF, **a**-**c**-**e**-**g**-**i**-**m**) and Windward Cold Facade (WCF, **b**-**d**-**f**-**h**-**l**-**n**) scenarios

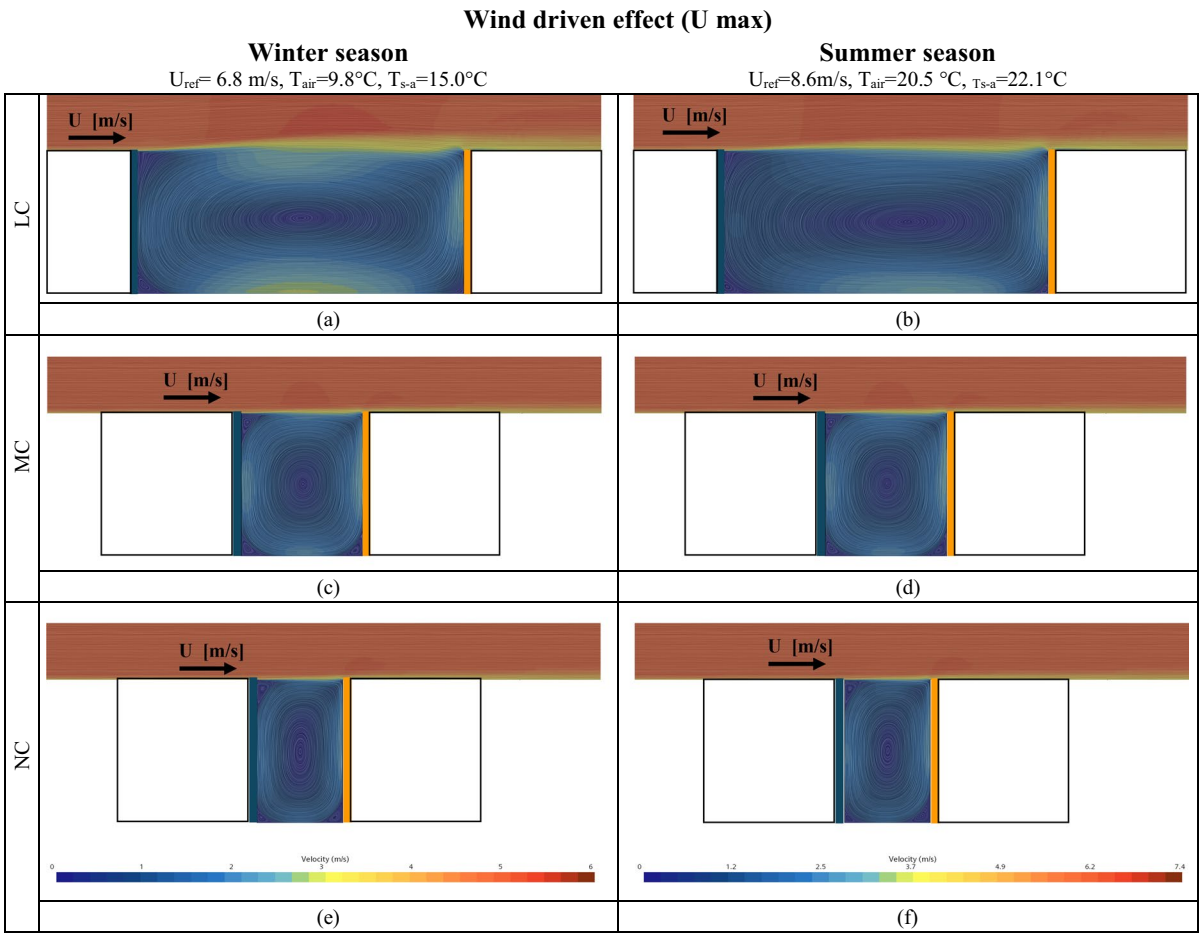

Fig. 14 **a**-**f**. Velocity field and vortical structures obtain from steady-state simulations, considering the extreme condition of the cross wind driven effect (Umax), in large (LC, **a**-**b**), medium (MC, **c**-**d**), and narrow (NC, **e**-**f**) canyons, in WWF scenarios, during the winter (**a**-**c**-**d**) and summer (**b**-**d**-**f**) seasons

vortex created inside the canyon, both circulating in the same direction.

Results of the 3-zones air flow model

In this paragraph are presented the results of the ach calculated for the case study building in the large (LC) and medium (MC) urban canyons. In both cases, the 3-zones air flow model is applied in 4 different climate scenarios of typical winter and summer days, both in windy and no-windy conditions. The two methodologies (*Cpmethod* and *CFDmethod*) have been applied to all scenarios and compared. The two methodologies differ for the calculation of the dynamic pressure p_{dyn} that directly depends on the wind velocity incident on both windward and leeward facades for all the external nodes (1, 2, 3, 4 in Fig. 9).

In the *Cpmethod* the incident wind velocity has been calculated, adjusting the reference wind velocity (U_{ref}) measured from the weather station according to the specific Cp evaluated at nodes' height (z).

In the *CFDmethod*, the incident wind velocity v_{CFD} (Table 13) is the results of the CFD analysis simulated separately for the large and medium canyons, extracted by the fitted curves (Fig. 16a-b) for each climate scenarios analyzed. For each of them, the associated equation that describes the velocity as a function of the quota has been directly used to determine the wind speed at the four height's nodes. Reference is made to the equation of probe 99% for the two nodes (1,2) in

Thermal gradient effect (I max)

	Winter season U_{ref}=2.1 m/s, T_{air}=8.5°C, T_{s-a}=31.5°C	**Summer season** U_{ref}=1.6m/s, T_{air}=20.5 °C, T_{s-a}=22.1°C
LC	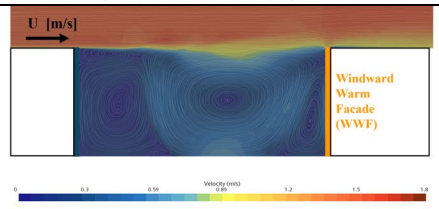	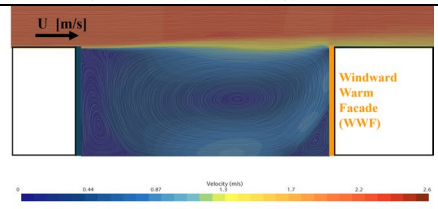
	(a)	(c)
	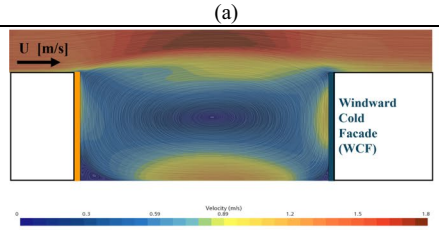	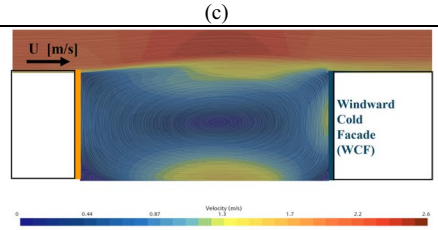
	(b)	(d)
MC	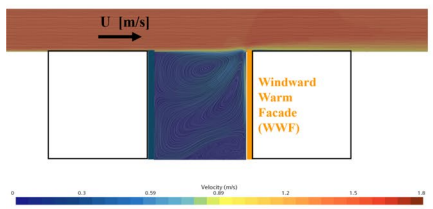	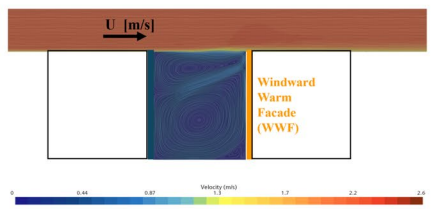
	(e)	(g)
	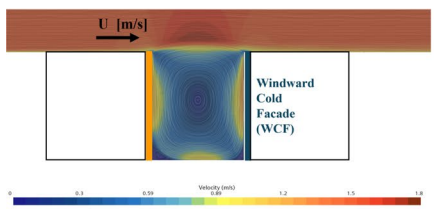	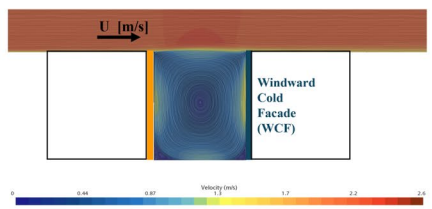
	(f)	(h)
NC	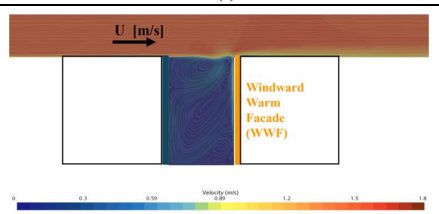	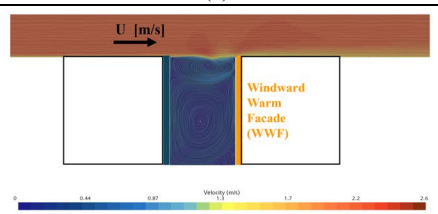
	(i)	(m)
	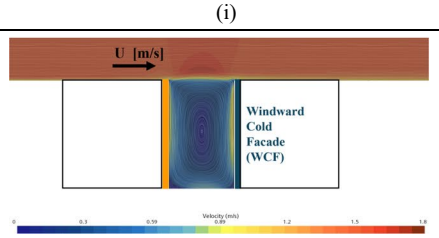	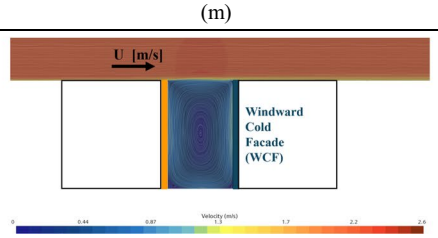
	(l)	(n)

◂**Fig. 15** **a**-**n**. Velocity field and vortical structures obtain from steady-state simulations, considering the extreme condition of the thermal gradient effect (Imax), in large (LC, **a**-**d**), medium (MC, **c**-**h**), and narrow (NC, **i**-**n**) canyons, during the winter (**a**-**b**-**e**-**f**-**i**-**l**) and summer (**c**-**d**-**g**-**h**-**m**-**n**) seasons, and Windward Warm Facade (WWF, **a**-**c**-**e**-**g**-**i**-**m**) and Windward Cold Facade (WCF, **b**-**d**-**f**-**h**-**l**-**n**) scenarios

the windward façade and to the equation of probe 1% for the two nodes (3,4) in the leeward façade.

For each external node (1,2,3,4) and in all the four climate scenarios, Table 13 presents the result of p_{dyn} at the nodes' height z on windward (WW) and leeward (LW) facades for both the large (LC) and medium (MC) canyons, comparing the *Cpmethod* and *CFDmethod*, according to Equation 14.1 and 14.2, respectively.

In both methodologies, all the p_{dyn} calculated at nodes (3,4) in the leeward (LW) façade have a negative sign related to the direction of the surface pressure. In all cases, p_{dyn} at low height (4.5m for nodes 1,3) is always lower than p_{dyn} at high height (13.5m for nodes 2,4), except the results of the CFD method for the leeward façade of the large canyon in the summer windy scenario (SUM-windy).

In all climate scenarios, p_{dynCFD} in the medium canyon (MC) is greater than p_{dynCFD} in the large canyon as shown in Fig. 16a-b, the vortex structure and the wind profile are similar for the 2 canyon dimensions, but in the MC the wind increases its magnitude. For this reason, in windy scenarios the increase is even more significant.

Comparing p_{dynCp} and p_{dynCFD}, they are of the same order of magnitude. The first is calculated only once, regardless of the size of the canyon, because it described pressure distribution along the façade at building scale. Therefore, for each scenario in Table 13, the same p_{dynCp} result can be compared with p_{dynCFD} of the large (LC) and medium (MC) canyons, and in both cases, it is always a lower value.

In windy scenarios, on the windward facade, the gap between p_{dynCp} calculated at the two nodes at different heights is significant: at a lower height (node 1) p_{dynCp} is always much lower than p_{dynCFD}, while at a higher height (node3) p_{dynCp} is always much greater than p_{dynCFD}. This is closely related to the value of the Cp coefficients (Table 13) for the windward façade (WW).

The *CFDmethod* is very sensitive to the height of the observed points (nodes) related to the dimensions of the canyon (LC and MC), as it considers the vortex created by the combined effect of the wind and thermal buoyancy. The *Cpmethod* overestimates the incident speed ($Cp \cdot U_{ref}^2$ in Table 13) on the facades because:

- it describes the surrounding built context through tabular values of parameters (PAD, SbH, roughness parameter) without considering neither the presence nor the geometry of the canyon,
- it only considers the effect of the incident wind and not the solar radiation which affects the convective motion of the air near the facades,
- the limited field of application of the table parameters makes it difficult to apply the Cpmethod to typical buildings in Turin (closed condominiums with a central garden courtyard).

The resulting air flow displacement through the building zones is the same for the two methods applied and for the two canyon dimensions (large and medium) analyzed; it is schematized in Fig. 17, considering the winter (Fig. 17a-b) and the summer seasons (Fig. 17c-d), in windy (Fig. 17a-c) and no wind (Fig. 17b-d) conditions. Here, the outdoor airflow (fresh air) is represented by a green arrow while the indoor airflow (exhausted air) is represented by a red arrow. In all climate scenarios, the incident wind on the windward façade let the outdoor air enters and pass through the heated zones, reaching the shaft. The only exception is the winter no windy scenario (Fig. 17b): at the upper level (node2) the air flows from the heated zone to the outdoor space, due to the poor wind condition and the prevalence of buoyancy effect.

Considering the shaft zone (node Pc), in all winter scenarios (Fig. 17a-b), the outdoor air enters from the ground level (node 3) and esc trough the leakages at higher level (node 4). In the summer scenarios it is the contrary: at the floor level (node 3) the air esc from the shaft, in both windy

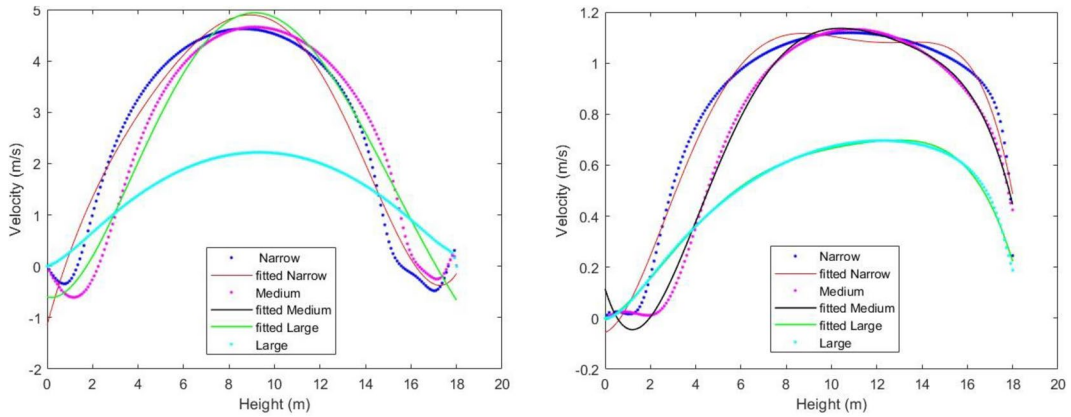

Fig. 16 a-b. Velocity field on windward façade (99%) for maximum conditions of wind-driven U max (**a**) and irradiation I_{inc} max (**b**) in the summer season WWF scenario, comparing the CFD results from the steady-state regime simulations (dotted lines) and the interpolated fitted curves with the fifth-grade polynomial function (straight lines), for the Narrow (blue dotted line), Medium (violet dotted line), and Large (green dotted line) canyons

(Fig. 17c) and no wind (Fig. 17d) scenarios. In the summer no wind scenario, the outdoor air enters from the higher leakages (node 4) in the shaft, while in the summer windy scenario, at the upper level the exhausted air esc from the shaft. In winter the external air is colder than the internal one, the

Table 13 Results of dynamic pressure p_{dyn} at the four external nodes' height, comparing Cp and CFD methods on windward (WW) and leeward (LW) facades of a large (LC) and medium (MC) canyons

Scenario		Large Canyon (LC)				Medium Canyon (MC)				
	Façade	WW		LW		WW		LW		
	Node	1	2	3	4	1	2	3	4	
	z	4.5	13.5	4.5	13.5	4.5	13.5	4.5	13.5	[m]
	Cp	0.005	0.223	-0.032	-0.041	0.005	0.223	-0.032	-0.041	[-]
WINT-windy (U_{ref} =5.0m/s)	$\mathbf{v_{CFD}}$	0.83	2.77	-0.17	-0.30	1.36	2.43	-1.06	-1.61	[ms^{-1}]
	$\mathbf{P_{dynCFD}}$	0.41	4.62	-0.02	-0.05	1.11	3.55	-0.67	-1.55	[Pa]
	$\mathbf{Cp \cdot U_{ref}^2}$	0.23	10.31	-1.48	-1.90	0.23	10.31	-1.48	-1.90	[m^2s^{-2}]
	$\mathbf{P_{dynCp}}$	0.14	6.25	-0.89	-1.14	0.14	6.25	-0.89	-1.14	[Pa]
WINT-no wind (U_{ref} =1.48 m/s)	$\mathbf{v_{CFD}}$	0.47	0.34	-0.17	-0.18	0.55	0.84	-0.36	-0.39	[ms^{-1}]
	$\mathbf{P_{dynCFD}}$	0.13	0.07	-0.02	-0.02	0.18	0.42	-0.08	-0.09	[Pa]
	$\mathbf{Cp \cdot U_{ref}^2}$	0.01	0.57	-0.08	-0.10	0.01	0.57	-0.08	-0.10	[m^2s^{-2}]
	$\mathbf{P_{dynCp}}$	0.00	0.34	-0.05	-0.07	0.00	0.34	-0.05	-0.07	[Pa]
SUM-windy (U_{ref}=6.17 m/s)	$\mathbf{v_{CFD}}$	2.06	3.20	-1.03	-1.70	2.31	3.51	-1.80	-2.68	[ms^{-1}]
	$\mathbf{P_{dynCFD}}$	2.54	6.14	-0.64	-1.73	3.21	7.38	-1.93	-4.30	[Pa]
	$\mathbf{Cp \cdot U_{ref}^2}$	0.37	16.50	-2.37	-3.03	0.37	16.50	-2.37	-3.03	[m^2s^{-2}]
	$\mathbf{P_{dynCp}}$	0.21	9.55	-1.37	-1.76	0.21	9.55	-1.37	-1.76	[Pa]
SUM-no wind (U_{ref} =2.18 m/s)	$\mathbf{v_{CFD}}$	0.75	1.13	-0.31	-0.57	0.87	1.32	-0.63	-1.14	[ms^{-1}]
	$\mathbf{P_{dynCFD}}$	0.34	0.85	-0.05	-0.26	0.45	1.05	-0.23	-0.78	[Pa]
	$\mathbf{Cp \cdot U_{ref}^2}$	0.01	0.57	-0.08	-0.10	0.01	0.57	-0.08	-0.10	[m^2s^{-2}]
	$\mathbf{P_{dynCp}}$	0.00	0.34	-0.05	-0.07	0.00	0.34	-0.05	-0.07	[Pa]

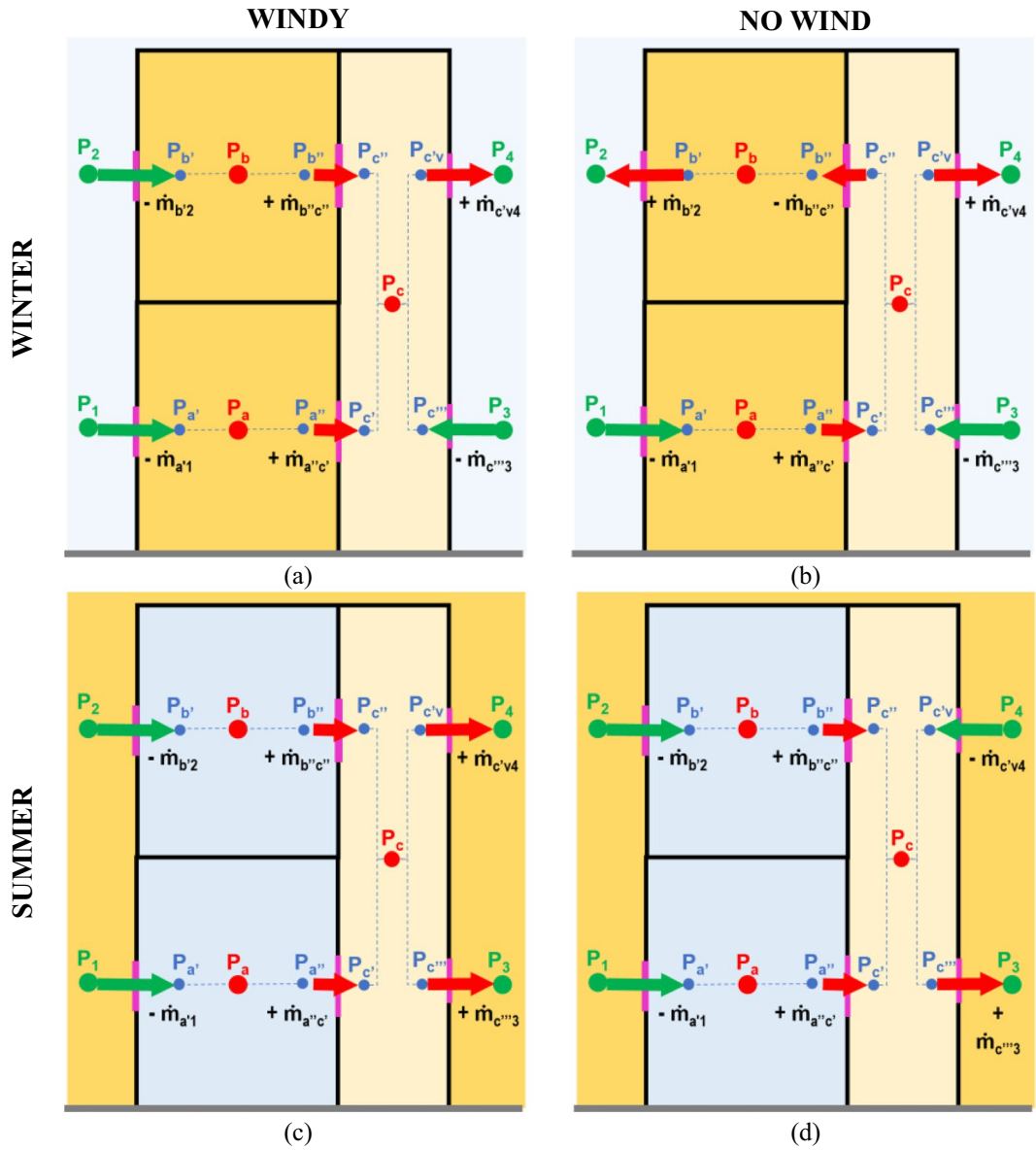

Fig. 17 **a**-**c**. Airflow displacement through buildings zones in both large (LC) and medium (MC) canyons, in winter-windy (**a**), winter-no wind (**b**), summer windy (**c**, only in MC) and summer no-wind (**d**) scenarios

warmer air in the shaft tends to rise, and it is possible to assume that the thermal buoyancy effect is predominant, vice versa in summer.

For all scenarios, in Table 14 are compared the results of the ach for each of the three zones of the building: the upper zone (b), the lower zone (a) and the shaft (c). The ach* is calculated considering all the airflow entering the zone: the outdoor fresh air and the recirculation air from internal zones. So, the ach* is always greater than the ach in the shaft (c).

The resulting ach values in each scenario are all lower than the fixed values used in the energy models (0.3-0.5), but this depends on the fact that this study only considers the airflow through the leakages of the openings. Considering only the results of the CFD method, in all zones the ach in the medium canyon (MC) is slightly greater

Table 14 Hourly ach [h^{-1}] for upper (b) and lower (a) heated zones and the shaft zone (c) in the building, comparing results of *Cp method* and *CFD method* for the large (LC) and medium (MC) canyons

Scenario	Method	Canyon	ach(a)	ach(b)	ach(c)	ach(c)*
WIN-windy	Cp	LC-MC	0.05	0.08	0.18	0.28
	CFD	LC	0.06	0.04	0.32	0.38
		MC	0.08	0.03	0.41	0.57
WIN-no wind	Cp	LC-MC	0.01	0.02	0.07	0.08
	CFD	LC	0.02	0.02	0.01	0.02
		MC	0.03	0.04	0.03	0.05
SUM- windy	Cp	LC-MC	0.03	0.10	0.07	0.20
	CFD	LC	0.06	0.07	0.28	0.42
		MC	0.06	0.12	-	0.18
SUM-no wind	Cp	LC-MC	0.01	0.02	0.13	0.16
	CFD	LC	0.01	0.03	0.06	0.09
		MC	0.05	0.15	0.08	0.11

* Outdoor airflow plus airflow from zones a and b

than the ones in the large canyon (LC), due to the increasing air velocity related to canyon dimension. For each scenario, the ach resulting from the Cp method can be compared with the ones of the CFD method for both LC and M: the values are of the same order of magnitude. In all scenarios, the ach at lower zones (a) is lower than the ach at upper level (b), except in winter windy climate scenario, for both the CFD method's application in large and medium canyons. In both winter and summer seasons the windy scenarios report higher ach values than the corresponding scenarios with no wind, due to the role of dynamic pressure in determining the passage of air in the areas of the building.

Table 15 reports the results (errors) of the three non-linear equations in the system Eq. (22a,b,c), considering the solutions of the iterative calculation. Errors closer to zero means that the solutions of the iterative calculation are more accurate and that the mass conservation law is verified in each node. The order of magnitude is similar between the various scenarios for the two methodologies applied.

Conclusion

In this work a three-zones air flow lumped model has been described and used to assess the hourly variation of the number of air changes per hour (ach).

Table 15 Errors of the three non-linear equations in the system Eq. (22a,b,c), corresponding to the mass conservation law balance at each node in the internal zones (a,b,c), comparing results of *Cp-method* and*CFD-method* for the the large (LC) and medium (MC) canyons

Scenario	Method	Canyon	Eq. 22a	Eq. 22b	Eq. 22c
WIN-windy	Cp	LC-MC	-0.004	-0.004	-0.024
	CFD	LC	0.000	0.000	-0.045
		MC	0.000	0.011	-0.077
WIN-no wind	Cp	LC-MC	0.002	0.008	0.040
	CFD	LC	-0.001	0.001	0.063
		MC	-0.003	0.008	0.059
SUM-windy	Cp	LC-MC	0.000	0.001	-0.039
	CFD	LC	0.000	0.000	-0.062
		MC	0.004	-0.007	0.065
SUM-no wind	Cp	LC-MC	-0.002	0.000	-0.033
	CFD	LC	-0.001	-0.003	-0.003
		MC	-0.008	-0.030	-0.023

The air displacement in a building is determined, considering only the air flow rate due to infiltrations, depending on leakages' characteristics and pressure variation due to the wind and buoyancy effect. The *fsolve* function has been used to solve the non-linear equations of mass conservation, through an iterative procedure.

The outdoor environmental condition of dynamic and static pressure on building façades have been determined by experimental values (Cp) and CFD simulations on urban canyons. Different climate scenarios have been considered to investigate the velocity field in the domain, evaluating the contributions of cross wind flow and thermal buoyancy in urban canyons with different dimensions. Then, polynomial function is interpolated to obtain the description of wind speed as function of the elevation.

The three-zones air flow lumped model can find the solutions with the numerical methodology for the case studies analyzed both with the Cp and the CFD outdoor data. The Cp data were used even if their field of application is not respected in environments with high building density. The CFD results can estimate the outside pressures and then airflow rates; in addition, it allows to modulate the ach at the building scale in different climatic scenarios, as the wind speed varies in relation to the canyon dimension and geometry.

Further developments of this work can improve the calculation of the outside pressures on buildings' facades at urban level. Finally, some progress could improve to match the numerical method with the physical-based modeling of space heating and cooling for the buildings within a city.

Acknowledgment Authors thank Prof. Franco Pellerey and his research group for their precious contribution in the definition of the numerical solution of air changes per hour modeling.

Declarations

Conflict of interest The authors have no conflict of interest.

References

Ai, Z. T., & Mak, C. M. (2017). CFD simulation of flow in a long street canyon under a perpendicular wind direction: Evaluation of three computational settings. *Building and Environment, 114*, 293–306. https://doi.org/10.1016/j.buildenv.2016.12.032

Ali, U., Shamsi, M. H., Hoare, C., Mangina, E., & O'Donnell, J. (2021). Review of urban building energy modeling (UBEM) approaches, methods and tools using qualitative and quantitative analysis. *Energy and Buildings, 246*. https://doi.org/10.1016/j.enbuild.2021.111073

Allard F., Herrlin M., (1989). Wind-Induced Ventilation - ASHRAE transactions, Air infiltration and Ventilation Centre (AIVC). https://www.aivc.org/sites/default/files/airbase_3534.pdf (accessed on June 17th, 2023).

Allegrini, J., Dorer, V., & Carmeliet, J. (2013). Wind tunnel measurements of buoyant flows in street canyons. *Building Environment, 59*, 315–326. https://doi.org/10.1016/j.buildenv.2012.08.029

Allegrini, J., Dorer, V., & Carmeliet, J. (2014). Buoyant flows in street canyons: Validation of CFD simulations with wind tunnel measurements. *Building Environment, 72*, 63–74. https://doi.org/10.1016/j.buildenv.2013.10.021

Bartak, M., et al. (2002). Integrating CFD and building simulation. *Building Environment, 37*(8-9), 865–871. https://doi.org/10.1016/S0360-1323(02)00045-8

Basu, S., Bale, C. S. E., Wehnert, T., & Topp, K. (2019). A complexity approach to defining urban energy systems. *Cities, 95*. https://doi.org/10.1016/j.cities.2019.05.027

Blocken, B., Janssen, W. D., & van Hooff, T. (2012). CFD simulation for pedestrian wind comfort and wind safety in urban areas: General decision framework and case study for the Eindhoven University campus. *Environmental Modelling & Software, 30*, 15–34. https://doi.org/10.1016/j.envsoft.2011.11.009

Calì M., Arena P., Borchiellini R., Mutani G. and. Vannelli G. (1997). Methods of analysis and verification of the performance of numerical codes aimed at energy and fluid dynamics calculations in civil and industrial buildings, Energy Dep. of Polytechnic of Turin, ITAG - Italian Technical Gas Association.

Di Bernardino, A., Monti, P., Leuzzi, G., & Querzoli, G. (2018). Pollutant fluxes in two-dimensional street canyons. *Urban Climate, 24*, 80–93. https://doi.org/10.1016/j.uclim.2018.02.002

Dols, W. S., & Polidoro, B. J. (2020). *CONTAM User Guide and Program Documentation Version 3.4*. National Institute of Standards and Technology. https://doi.org/10.6028/NIST.TN.1887r1

Feustel H. E., (2013). TN 29: Fundamentals of the Multizone Air Flow Model- COMIS, in AIVC. https://www.aivc.org/resource/tn-29-fundamentals-multizone-air-flow-model-comis (access on June 13th, 2023).

Harish, V. S. K. V., & Kumar, A. (2016). A review on modeling and simulation of building energy systems. *Renewable and Sustainable Energy Reviews, 56*. https://doi.org/10.1016/j.rser.2015.12.040

Hassan, M. A., Khalil, A., & Abubakr, M. (2021). Selection methodology of representative meteorological days for assessment of renewable energy systems. *Renewable Energy, 177*. https://doi.org/10.1016/j.renene.2021.05.124

Javanroodi, K., Nik, V. M., Giometto, M. G., & Scartezzini, J.-L. (2022). Combining computational fluid dynamics and neural networks to characterize microclimate extremes: Learning the complex interactions between meso-climate and urban morphology. *Science of the Total Environment, 829*. https://doi.org/10.1016/j.scitotenv.2022.154223

Lenin, G., Krishnan, P. E., & Ramkumar, R. (2022). Effect of various parameters on sol-air temperature. *International Journal of Mechanical Engineering*.

Li, X.-X., Britter, R. E., Norford, L. K., Koh, T.-Y., & Entekhabi, D. (2012). Flow and Pollutant Transport in Urban Street Canyons of Different Aspect Ratios with Ground Heating: Large-Eddy Simulation. *Boundary-Layer Meteorology, 142-2*, 289–304. https://doi.org/10.1007/s10546-011-9670-9

Mckeen, P., & Liao, Z. (2019). The Influence of Building Airtightness on Airflow in Stairwells. *Buildings, 9*(10), 10. https://doi.org/10.3390/buildings9100208

Mouzourides, P., Marakkos, C., & Neophytou, M. K.-A. (2022). Urban street canyon flows under combined wind forcing and thermal buoyancy. *Physics of Fluids*, 34–37. https://doi.org/10.1063/5.0090642

Mun, J., Lee, J., & Kim, M. (2021). Estimation of Infiltration Rate (ACH Natural) Using Blower Door Test and Simulation. *Energies, 14*(4), 4. https://doi.org/10.3390/en14040912

Mutani G., Santantonio S., and Todeschi V., (2021). Evaluation of ventilation loads in buildings energy modelling at urban scale, in 2021 IEEE 4th International Conference and Workshop Óbuda on Electrical and Power Engineering (CANDO-EPE). doi: https://doi.org/10.1109/CANDO-EPE54223.2021.9667547.

Mutani, G., & Todeschi, V. (2020). Building energy modeling at neighborhood scale. *Energy Efficiency, 13-7*, 1353–1386. https://doi.org/10.1007/s12053-020-09882-4

Mutani, G., Vocale, P., & Javanroodi, K. (2023). Toward Improved Urban Building Energy Modeling Using a Place-Based Approach. *Energies, 16*(9), 9. https://doi.org/10.3390/en16093944

Najafi, Z. N., Cook, M., & O'Sullivan, P. D. (2023). The effect of airflow guiding components on effective ventilation rates in single-sided ventilation applications. *International Journal of Ventilation*. https://doi.org/10.1080/14733315.2023.2198793

O'Neill, J. J., Cai, X.-M., & Kinnersley, R. (2016). Stochastic backscatter modelling for the prediction of pollutant removal from an urban street canyon: A large-eddy simulation. *Atmospheric Environment, 142*, 9–18. https://doi.org/10.1016/j.atmosenv.2016.07.024

Palusci, O., & Cecere, C. (2022). Urban Ventilation in the Compact City: A Critical Review and a Multidisciplinary Methodology for Improving Sustainability and Resilience in Urban Areas. *Sustainability, 14*(7), 3948. https://doi.org/10.3390/su14073948

Palusci, O., Monti, P., Cecere, C., Montazeri, H., & Blocken, B. (2022). Impact of morphological parameters on urban ventilation in compact cities: The case of the Tuscolano-Don Bosco district in Rome. *Science of the Total Environment, 807*. https://doi.org/10.1016/j.scitotenv.2021.150490

Perera, A. T. D., Javanroodi, K., Wang, Y., & Hong, T. (2021). Urban cells: Extending the energy hub concept to facilitate sector and spatial coupling. *Advances in Applied Energy, 3*. https://doi.org/10.1016/j.adapen.2021.100046

Perera, A. T. D., et al. (2023). Challenges resulting from urban density and climate change for the EU energy transition. *Nature Energy, 8*(4), 4. https://doi.org/10.1038/s41560-023-01232-9

Rezaeiha, A., Montazeri, H., & Blocken, B. (2020). A framework for preliminary large-scale urban wind energy potential assessment: Roof-mounted wind turbines. *Energy Conversion and Management, 214*. https://doi.org/10.1016/j.enconman.2020.112770

Samsonov, T., Konstantinov, P., & Varentsov, M. (2015). Object-oriented approach to urban canyon analysis and its applications in meteorological modeling. *Urban Climate, 13*. https://doi.org/10.1016/j.uclim.2015.07.007

Sanaieian, H., Tenpierik, M., van den Linden, K., Mehdizadeh, S. F., & Majid Mofidi Shemrani, S. (2014). Review of the impact of urban block form on thermal performance, solar access and ventilation. *Renewable and Sustainable Energy Reviews, 38*, 551–560. https://doi.org/10.1016/j.rser.2014.06.007

Santantonio S. and Mutani G., (2022). QGIS-based tools to evaluate air flow rate by natural ventilation in buildings at urban scale, in 5th Building Simulation Applications Conference (BSA 2022), Proceedings ISSN 2531-6702, Bolzen (IT), June 29th – July 1st 2022, doi: https://doi.org/10.13124/9788860461919.

Toparlar, Y., Blocken, B., Maiheu, B., & van Heijst, G. J. F. (2017). A review on the CFD analysis of urban microclimate. *Renewable and Sustainable Energy Reviews, 80*, 1613–1640. https://doi.org/10.1016/j.rser.2017.05.248

Tsichritzis, L., & Nikolopoulou, M. (2019). The effect of building height and façade area ratio on pedestrian wind comfort of London. *Journal of Wind Engineering and Industrial Aerodynamics, 191*, 63–75. https://doi.org/10.1016/j.jweia.2019.05.021